Interfering with VE-PTP stabilizes endothelial junctions in vivo via Tie-2 in the absence of VE-cadherin

Maike Frye,[1]* Martina Dierkes,[1]* Verena Küppers,[1] Matthias Vockel,[1] Janina Tomm,[1] Dagmar Zeuschner,[2] Jan Rossaint,[4] Alexander Zarbock,[4] Gou Young Koh,[5,6] Kevin Peters,[3] Astrid Fee Nottebaum,[1] and Dietmar Vestweber[1]

[1]Max Planck Institute for Molecular Biomedicine, D-48149 Münster, Germany
[2]Electron Microscopy Unit, Max Planck Institute for Molecular Biomedicine, D-48149 Münster, Germany
[3]Aerpio Therapeutics, Cincinnati, OH 45242
[4]Department of Anesthesiology and Critical Care Medicine, University of Münster, D-48149 Münster, Germany
[5]Center for Vascular Research, Institute of Basic Science and [6]Graduate School of Medical Science and Engineering, Korea Advanced Institute of Science and Technology, Daejeon 305-701, Republic of Korea

The Journal of Experimental Medicine

Vascular endothelial (VE)–protein tyrosine phosphatase (PTP) associates with VE-cadherin, thereby supporting its adhesive activity and endothelial junction integrity. VE-PTP also associates with Tie-2, dampening the tyrosine kinase activity of this receptor that can support stabilization of endothelial junctions. Here, we have analyzed how interference with VE-PTP affects the stability of endothelial junctions in vivo. Blocking VE-PTP by antibodies, a specific pharmacological inhibitor (AKB-9778), and gene ablation counteracted vascular leak induction by inflammatory mediators. In addition, leukocyte transmigration through the endothelial barrier was attenuated. Interference with Tie-2 expression in vivo reversed junction-stabilizing effects of AKB-9778 into junction-destabilizing effects. Furthermore, lack of Tie-2 was sufficient to weaken the vessel barrier. Mechanistically, inhibition of VE-PTP stabilized endothelial junctions via Tie-2, which triggered activation of Rap1, which then caused the dissolution of radial stress fibers via Rac1 and suppression of nonmuscle myosin II. Remarkably, VE-cadherin gene ablation did not abolish the junction-stabilizing effect of the VE-PTP inhibitor. Collectively, we conclude that inhibition of VE-PTP stabilizes challenged endothelial junctions in vivo via Tie-2 by a VE-cadherin–independent mechanism. In the absence of Tie-2, however, VE-PTP inhibition destabilizes endothelial barrier integrity in agreement with the VE-cadherin–supportive effect of VE-PTP.

The endothelium of the blood vessel wall forms a barrier for blood solutes and for leukocytes. The entry of molecules and cells of the immune system into inflamed tissue is mainly regulated via endothelial junctions. Vascular endothelial (VE)–cadherin is a central component of these junctions, and it is generally considered one of the major adhesive mechanisms that controls the stability and barrier function of the endothelium (Dejana and Vestweber, 2013). Antibodies against VE-cadherin can destabilize endothelial junctions in vitro and in vivo (Breviario et al., 1995; Gotsch et al., 1997; Corada et al., 1999). In agreement with this, enhancing the adhesive function of VE-cadherin by directly fusing it to α-catenin blocks the induction of vascular permeability in the skin of the respective knock-in mice and strongly reduces leukocyte extravasation in various tissues (Schulte et al., 2011).

The VE–protein tyrosine phosphatase (PTP) was shown to associate with VE-cadherin and thereby enhance the adhesive function of VE-cadherin (Nawroth et al., 2002; Nottebaum et al., 2008). Permeability-inducing mediators such as VE growth factor (VEGF) and the attachment of leukocytes to endothelial cells (ECs) both stimulate a signaling pathway that triggers the dissociation of VE-PTP from VE-cadherin (Nottebaum et al., 2008; Vockel and Vestweber, 2013). This dissociation is necessary for the induction of vascular permeability and for leukocyte extravasation in vivo. Evidence for this has been based on the analysis of knock-in mice where modified forms of VE-cadherin and VE-PTP, each containing a different binding site for a small molecular weight compound, had been knocked into the VE-cadherin locus (Broermann et al., 2011). In these mice, administration of the appropriate compound inhibited the dissociation of VE-PTP from VE-cadherin and thereby attenuated the induction of vascular permeability and leukocyte extravasation, demonstrating the importance of VE-cadherin–associated VE-PTP for the control of endothelial junction stability in vivo. Moreover, HIF2α was recently reported to enhance endothelial barrier

*M. Frye and M. Dierkes contributed equally to this paper.

Correspondence to Dietmar Vestweber: vestweb@mpi-muenster.mpg.de

Abbreviations used: BBB, blood–brain barrier; Comp, cartilage oligomeric matrix protein; EC, endothelial cell; MLC, myosin light chain; PTP, protein tyrosine phosphatase; VE, vascular endothelial; VEGF, VE growth factor.

The Rockefeller University Press $30.00
J. Exp. Med. 2015 Vol. 212 No. 13 2267–2287
www.jem.org/cgi/doi/10.1084/jem.20150718

integrity, in part through induced VE-PTP expression (Gong et al., 2015). In line with these findings, tyrosine phosphorylation of VE-cadherin has been demonstrated to be involved in the regulation of EC contacts in vitro (Allingham et al., 2007; Turowski et al., 2008; Monaghan-Benson and Burridge, 2009) and in vivo (Orsenigo et al., 2012; Wessel et al., 2014).

VE-PTP also associates with Tie-2 (Fachinger et al., 1999), an endothelial tyrosine kinase receptor that regulates angiogenesis and can support the integrity of endothelial junctions. VE-PTP gene ablation causes embryonic lethality at embryonic day (E) 9.5 (Bäumer et al., 2006; Dominguez et al., 2007). This is caused by a defect in blood vessel remodeling leading to enlarged and fused vessel structures. Antibodies against VE-PTP caused similar defects when incubated with explant cultures of allantois from WT mice, but not if the tissue originated from Tie-2 gene–deficient mice (Winderlich et al., 2009). In addition, these antibodies against the extracellular part of VE-PTP dissociated the phosphatase from Tie-2 and caused phosphorylation of this receptor and signaling (Winderlich et al., 2009).

We have recently shown that a specific pharmacological inhibitor of VE-PTP catalytic activity, AKB-9778, activated Tie-2 in the mouse, and this correlated with suppression of ocular neovascularization and blocking of VEGF-induced vascular leak (Shen et al., 2014). Although direct evidence for the relevance of Tie-2 is still missing, these results are in line with studies reporting that the Tie-2 ligand Angiopoietin-1 (Ang1) protects the vasculature against plasma leakage (Gamble et al., 2000; Thurston et al., 2000; Mammoto et al., 2007; Gavard et al., 2008). In a mouse breast cancer model, AKB-9778 normalized tumor vessels and delayed tumor growth (Goel et al., 2013). VE-PTP was also found to associate with VEGF receptor-2 (VEGFR-2; Mellberg et al., 2009), and this interaction was suggested to affect VEGFR-2 activity in endothelial sprouts of mouse embryoid bodies (Hayashi et al., 2013).

Here we have analyzed how interference with VE-PTP activity influences endothelial junctions in adult mice and how this relates to the functions of Tie-2 and VE-cadherin. We found that conditional gene ablation of VE-PTP, as well as interference with antibodies or administering the inhibitor AKB-9778 each stabilized challenged endothelial junctions, thereby preventing enhanced permeability and leukocyte extravasation induced by inflammatory mediators. These effects required the expression of Tie-2 because blocking its expression in vivo reversed the effect of the VE-PTP inhibitor on endothelial junction integrity. Thus, VE-PTP inhibition stabilizes challenged endothelial junctions via Tie-2 and destabilizes them in the absence of Tie-2. Remarkably, the junction-stabilizing effect was even observed in mice conditionally gene deficient for VE-cadherin. Inhibition of leak formation was accompanied by activation of Rap1 and cytoskeletal remodeling and reduced radial stress fiber formation. Our results reveal that inhibition of VE-PTP in vivo has opposing effects on endothelial junctions as the result of its different effects on VE-cadherin and on Tie-2. Activation of Tie-2 via inhibition of VE-PTP protects endothelial junctions against inflammation-induced destabilization and overrides the negative effect of VE-PTP inhibition on the adhesive function of VE-cadherin.

RESULTS

Interference with VE-PTP by independent approaches stabilizes the endothelial barrier

We have recently shown that a pharmacological phosphatase inhibitor with high specificity for VE-PTP, AKB-9778, counteracts VEGF-induced permeability across HUVEC monolayers and VEGF- and histamine-induced vascular permeability in the skin of mice in a classical Miles assay (Shen et al., 2014). To verify whether these effects were indeed caused by the inhibition of VE-PTP and no other phosphatases, here we tested whether affinity-purified pAbs against the extracellular part of VE-PTP would have similar effects. HUVEC monolayers grown on transwell filters were preincubated either with control antibodies from preimmune serum or with affinity-purified antibodies against VE-PTP, followed by the incubation with or without the permeability-inducing reagent. As shown in Fig. 1 (A and B), the substantial increase of permeability for 250-kD FITC-dextran, induced by thrombin or VEGF, was efficiently reduced with anti–VE-PTP antibodies. Similar results were obtained when we replaced the antibody treatment by incubation with 10 µM AKB-9778 for 30 min, whereas vehicle alone had no effect (Fig. 1 C). Both of these independent methods of VE-PTP inhibition induced tyrosine phosphorylation of the VE-PTP substrate Tie-2 (Fig. 1 D).

To test whether antibodies against the extracellular domain of VE-PTP would also stabilize the endothelial barrier in vivo, we performed a Miles assay in C57BL/6 mice. Upon i.v. administration of 200 µg of affinity-purified anti–VE-PTP antibodies or control antibodies, Evans blue was i.v. injected 30 min after antibody administration, and the skin was challenged 10 min later by intradermal injection of either PBS or VEGF (25 ng in 50 µl). Anti–VE-PTP antibodies blocked VEGF-induced vascular permeability by 55% (±7%; Fig. 1 E). In the same mice, the anti–VE-PTP antibody treatment stimulated tyrosine phosphorylation of Tie-2, as seen in immunoblots of Tie-2 that was immunoprecipitated from lung lysates (Fig. 1 F). Collectively, these results show that inhibiting VE-PTP with antibodies or with a small molecule inhibitor counteracts destabilization of EC contacts in vitro and in vivo, an effect that correlates with the activation of Tie-2.

VE-PTP gene ablation counteracts inflammation-induced vascular permeability

To analyze the relevance of VE-PTP for the integrity of endothelial junctions in vivo independent of pharmacologic inhibitors, we analyzed mice with an inactivated *Ptprb* gene. Because this gene is essential for embryonic development (Bäumer et al., 2006; Dominguez et al., 2007), we generated mice with exon 20 of the *Ptprb* gene flanked by loxP sites (Fig. 2 A). Cre-mediated excision of exon 20 was predicted

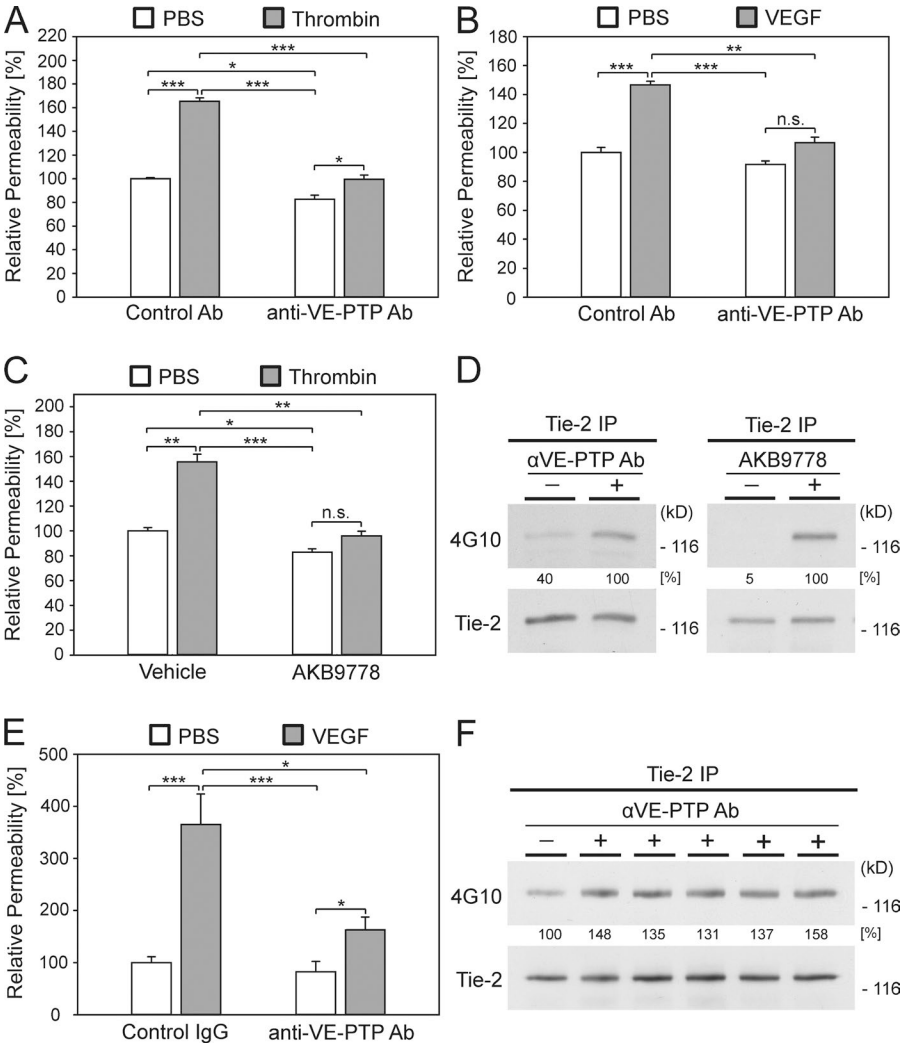

Figure 1. **Inhibiting VE-PTP reinforces endothelial barrier stability in vitro and in vivo.** (A–C) Paracellular permeability for 250-kD FITC-dextran was determined for HUV EC monolayers grown on transwell filters. Permeability was induced either with thrombin (A and C) or with VEGF (B; as indicated). Permeability of PBS-treated cells was set to 100%. For VE-PTP targeting, cells were either treated with anti–VE-PTP pAbs (A and B) or with the VE-PTP inhibitor AKB-9778 (C; as indicated). As a control, cells were treated with preimmune antibodies (control Ab) or solvent alone (vehicle). (D) Tie-2 was immunoprecipitated from either untreated (–) or anti–VE-PTP antibody (αVE-PTP Ab)– or AKB-9778–treated HUVECs (as indicated) and immunoblotted for anti–phospho-tyrosine (4G10) or anti–Tie-2 (Tie-2). (E) Mice were injected i.v. with control IgG or anti-VEPTP antibodies (as indicated). 30 min before the start of the Miles assay, Evans blue was i.v. injected, followed by intradermal injection of VEGF or PBS (as indicated) 10 min later. After 30 min, mice were sacrificed, and the dye was extracted from skin samples and quantified. (F) Tie-2 was immunoprecipitated from lung lysates of either control IgG (–)– or anti–VE-PTP antibody–injected mice and immunoblotted as in D. Data are pooled from three independent experiments with three replicates in each experiment (A–C) or two independent experiments with four to five mice per group in each experiment (E). Statistical significance was analyzed using the one-way ANOVA test, and for D the Mann-Whitney rank sum test was used. *, $P \leq 0.05$; **, $P \leq 0.01$; ***, $P \leq 0.001$. Results are shown as means ± SEM.

to cause a truncation of the VE-PTP protein within the 17th fibronectin type III–like repeat of the extracellular domain because deletion of exon 20 creates an in-frame stop codon at the start of exon 21. As a consequence, this would remove the transmembrane and the catalytic domain of the phosphatase. Southern blot analysis of DNA of the generated mice with an external probe (not depicted) as well as PCR genotyping revealed the expected results (Fig. 2 B). To confirm that Cre excision of exon 20 results in a functional *Ptprb*-null allele, mice were bred to a *Pgk-Cre* driver line that expressed Cre recombinase at the one-cell embryo stage. Homozygous deletion resulted in embryonic lethality at E9.5 (not depicted), similar as shown before for gene-deficient mice where either exon 18 (Bäumer et al., 2006) or exon 1 (Dominguez et al., 2007) had been constitutively deleted.

To inactivate *Ptprb* in postnatal ECs, $Ptprb^{lox/lox}$ mice were bred to tamoxifen-inducible *Pdgfb-iCre* transgenics. To test the effect of Cre-induced deletion on VE-PTP protein expression, we performed immunoblots of primary ECs isolated from the lungs of $Pdgfb\text{-}iCre^{+}$, $Ptprb^{lox/lox}$ ($Ptprb^{iECKO}$) mutants that had been repeatedly treated by i.p. injections of tamoxifen. pAbs against the first eight FN type III–like repeats of the extracellular part of VE-PTP recognized VE-PTP in immunoblots of cell lysates of ECs from WT mice but did not detect a truncated form of VE-PTP in lysates of ECs of the mutant mice (Fig. 2 C). Likewise, no truncated form of VE-PTP was detected in culture supernatants of these cells (Fig. 2 D). Thus, if the expectable truncated form of VE-PTP was expressed, it was most likely unstable. In agreement with this, VE-PTP was not detectable by FACS on primary ECs of these mice (not depicted).

To determine whether VE-PTP gene ablation would influence the integrity of endothelial junctions, we performed a Miles assay with WT mice and $Ptprb^{iECKO}$ mutants. Based on i.v. injected Evans blue and intradermal challenge with VEGF or histamine, we found that permeability induction was clearly reduced in tamoxifen-treated $Ptprb^{iECKO}$ mice (Fig. 2 E). Immunoblots of lung lysates of these mice probed with antibodies against the extracellular part of VE-PTP revealed that Cre-induced gene ablation resulted in the loss of most of the VE-PTP

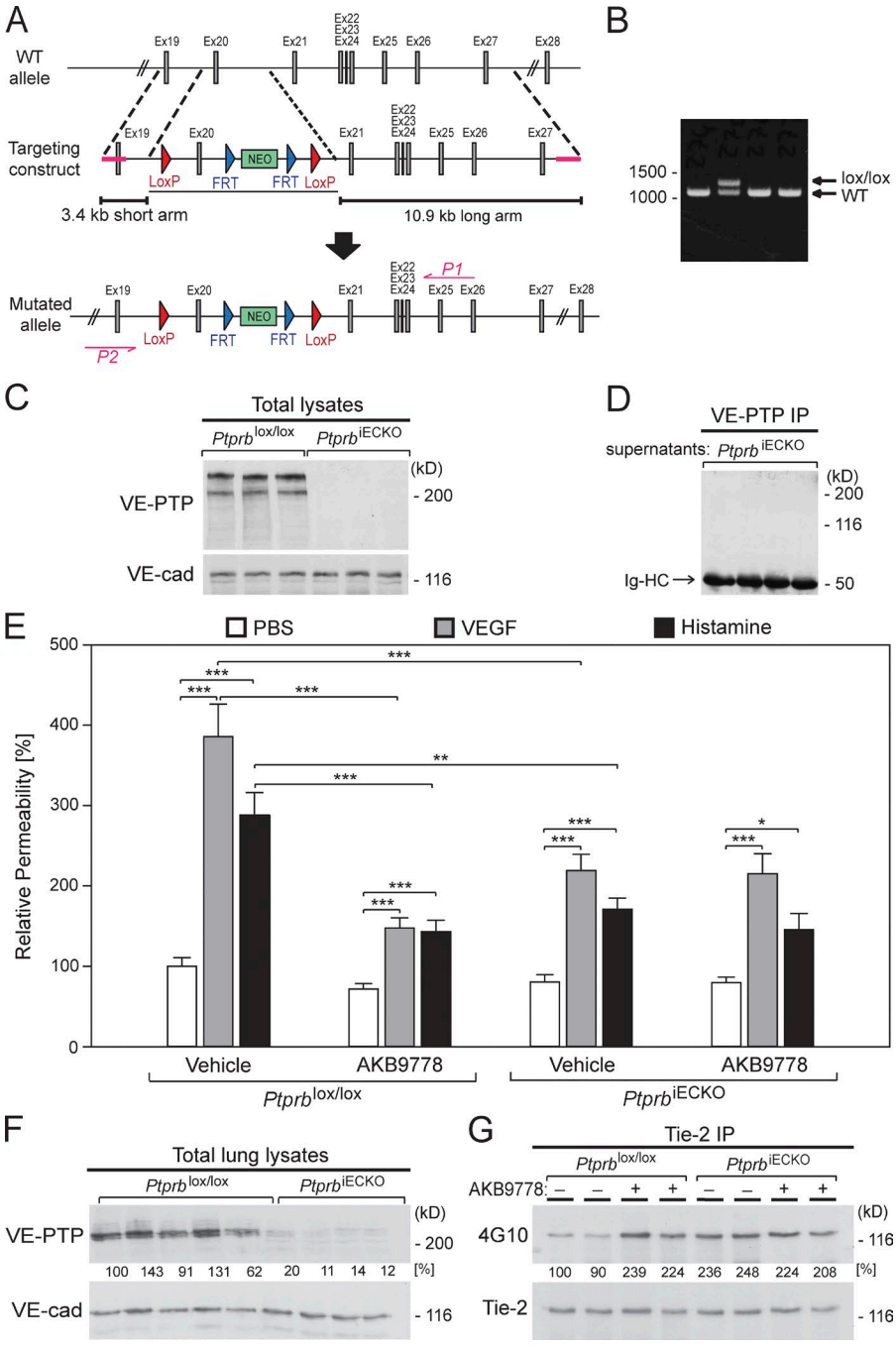

Figure 2. **Conditional *Ptprb* gene inactivation in mice and analysis of its effect on vascular permeability.** (A) A map of the relevant genomic region is shown, containing exon 20, flanked by loxP sites. Gene inactivation creates a stop codon at the start of exon 21 that codes for the transmembrane domain of VE-PTP. (B) PCR genotyping using primers P1 and P2 resulted in 1,440-bp or 1,290-bp products for the mutant or WT allele, respectively. (C and D) Immunoblots of VE-PTP of cell lysates (C) and of VE-PTP immunoprecipitates of culture supernatants (D) of primary ECs isolated from lungs of either $Ptprb^{lox/lox}$ or of $Ptprb^{iECKO}$ mice (as indicated), each treated repeatedly with i.p. injected tamoxifen. Blots were incubated with pAbs against the extracellular domain of VE-PTP or antibodies against VE-cadherin (as indicated; Ig-HC, IgG heavy chain). (E) $Ptprb^{lox/lox}$ or $Ptprb^{iECKO}$ mice were i.p. injected with tamoxifen daily for 5 d. 5 d later, mice were either subcutaneously injected with AKB-9778 or with vehicle (as indicated), and 30 min later, Evans blue was i.v. injected, followed by intradermal injection of PBS, VEGF, or histamine (as indicated) 10 min later. After 30 min, mice were sacrificed, and the dye was extracted from skin samples and quantified. (F and G) Total lung lysates (F) or Tie-2 immunoprecipitates (G) of mice from E were immunoblotted for VE-PTP or VE-cadherin (F) or for phospho-tyrosine (4G10) or Tie-2 (G) as indicated. Data are representative of at least two independent experiments (C, D, F, and G) and pooled from two independent experiments with four mice per group in each experiment (E). Statistical significance was analyzed using the one-way ANOVA test. *, $P \leq 0.05$; **, $P \leq 0.01$; ***, $P \leq 0.001$. Results are shown as means ± SEM.

protein (Fig. 2 F). Strong inhibition of VEGF- and histamine-induced vascular permeability was also seen with the VE-PTP inhibitor AKB-9778 (24 mg/kg) in WT mice (Fig. 2 E), whereas it had no additional inhibitory effect on the induction of vascular permeability in $Ptprb^{iECKO}$ mice, confirming the high specificity of the inhibitor for VE-PTP (Fig. 2 E). In agreement with these results, VE-PTP deletion and the VE-PTP inhibitor both enhanced Tie-2 phosphorylation in vivo, as determined in phospho-tyrosine blots of Tie-2, immunoprecipitated from lung lysates (Fig. 2 G). Again, the inhibitor had no additive effect on Tie-2 phosphorylation in $Ptprb^{iECKO}$ mice (Fig. 2 G). These results demonstrate that the phosphatase inhibitor AKB-9778 stabilizes challenged EC contacts and activates Tie-2 in vivo selectively via VE-PTP. Collectively, these results indicate that pharmacologic inhibition or genetic ablation of VE-PTP counteracts destabilization of EC contacts.

VE-PTP inhibition stabilizes endothelial junctions via Tie-2

Because pharmacologic inhibition and genetic ablation of VE-PTP both stabilize endothelial barrier integrity and in-

crease the phosphorylation of Tie-2, we asked whether Tie-2 is required for the junction-stabilizing effect of the inhibitor. Therefore, we transfected HUVECs with Tie-2 siRNA or control siRNA and tested the effect of 10 µM AKB-9778 or vehicle alone on thrombin-induced permeability of monolayers of these cells for FITC-dextran. As shown in Fig. 3 A, AKB-9778 blocked thrombin-induced permeability under control siRNA conditions, whereas this effect was no longer observed if Tie-2 expression was inhibited by siRNA. The expression of Tie-2 was inhibited by the siRNA treatment by 86%, and no effect was seen for VE-PTP or VE-cadherin (Fig. 3 C). Thus, the stabilizing effect of AKB-9778 on endothelial junctions depends on Tie-2.

When similar experiments were performed without thrombin treatment, we found that baseline permeability of HUVEC monolayers was not affected by AKB-9778 if Tie-2 was still expressed (control siRNA), whereas the inhibitor enhanced permeability if Tie-2 expression was reduced (Fig. 3 B). The fact that AKB-9778 did not affect baseline permeability when Tie-2 was still expressed prompted us to test the effect of AKB-9778 and cartilage oligomeric matrix protein (Comp)–Ang1 on baseline permeability of confluent HUVECs at different densities. We found clear inhibitory effects with AKB-9778 on confluent monolayers of cells seeded at 2.7-fold lower cell density, whereas the effect was lost at higher cell density (4.5×10^4 cells/cm^2 vs. 1.2×10^5 cells/cm^2 grown for 54 h; Fig. 3 D). Because VE-PTP junctional expression and association with VE-cadherin are weak at low cell density and increase with higher confluence (Nottebaum et al., 2008), we assume that only at high confluence the AKB-9778 effect on VE-cadherin compensates the effect on Tie-2, whereas at lower confluence the effect via Tie-2 is dominant. In agreement with this, Comp-Ang1 inhibited permeability at both levels of confluence (Fig. 3 D).

In line with previously published Tie-2 silencing experiments (Hakanpaa et al., 2015), inhibition of Tie-2 expression alone resulted in increased endothelial permeability (Fig. 3 B), suggesting that Tie-2 is necessary for cell contact integrity. Mechanistically, Tie-2 may support junction integrity by counteracting Ang-2–integrin signaling, which destabilizes cell contacts (Hakanpaa et al., 2015). In addition, the intrinsic kinase activity of Tie-2 may be responsible for reinforcing cell contact integrity.

The junction-destabilizing effect of AKB-9778 in the absence of Tie-2 is in line with the supportive effect of VE-PTP for VE-cadherin (Nottebaum et al., 2008; Broermann et al., 2011). Potential VE-PTP substrates that are responsible for this effect are VE-cadherin–Y685 and plakoglobin (Nottebaum et al., 2008; Wessel et al., 2014), and both are phosphorylated after AKB-9778 treatment of ECs (not depicted). Other candidates would be VEGFR-2 (Hayashi et al., 2013) or Src, which are both relevant for the phosphorylation of VE-cadherin. To test this, we either transfected HUVECs with control siRNA or with Tie-2 siRNA and treated the cells with either vehicle alone or 5 µM AKB-9778 for 30 min, followed by immunoprecipitation of VEGFR-2 or Src and immunoblotting either for phospho-tyrosine or for Src-pY418. As shown in Fig. 3 (E and G), AKB-9778 induced VEGFR-2 tyrosine phosphorylation independent of the expression of Tie-2 but had no significant effect on Src phosphorylation. VEGF induced the phosphorylation of VEGFR-2 slightly more efficiently than AKB-9778 (Fig. 3 F).

To test whether Tie-2 is also responsible for the junction-stabilizing effect of AKB-9778 in vivo, we inhibited the expression of Tie-2 in mice by in vivo siRNA using a polyethyleneimine-based transfection reagent (in vivo-jetPEI). As shown in Fig. 3 J, i.v. injection of Tie-2 siRNA could efficiently block the expression of Tie-2, as was analyzed by immunoblotting of lung lysates. Quantification of immunoblot signals for 13 control and 12 Tie-2 siRNA–treated mice revealed 74% (±4%) reduction of Tie-2 expression (Fig. 4 G). Mice treated with the transfection reagent in combination either with control siRNA or with a Tie-2 siRNA were analyzed for basal (Fig. 3 H) and for LPS-induced vascular permeability in the lung (Fig. 3 I). For LPS challenge, mice were exposed to aerosolized LPS for 40 min, and vascular permeability was determined by injecting Evans blue 4 h later for 15 min. As shown in Fig. 3 H, AKB-9778 had no effect on baseline vascular permeability when Tie-2 was expressed (ctrl siRNA condition). In contrast, Tie-2 siRNA treatment enhanced vascular permeability slightly (by 27 ± 10%), and administering AKB-9778 in addition enhanced permeability by an additional 43% (±13%; Fig. 3 H). LPS-induced permeability in mice expressing normal levels of Tie-2 (ctrl siRNA) could be clearly counteracted with the AKB-9778 inhibitor, whereas LPS-induced permeability in Tie-2 siRNA–treated mice could no longer be inhibited with this compound (Fig. 3 I). Thus, in analogy to the in vitro results, Tie-2 expression was required for the protective effect of AKB-9778 on inflammation-induced vascular permeability in the lung. Furthermore, under baseline conditions, inhibiting the expression of Tie-2 reverts the junction-stabilizing effect of the VE-PTP inhibitor into a junction-destabilizing effect (Fig. 3, B and H). Finally, Tie-2 expression is essential for baseline integrity of the blood vessel wall.

Inhibition of VE-PTP impedes transendothelial migration of leukocytes via activation of Tie-2

The stabilizing effect of the VE-PTP inhibitor AKB-9778 on EC junctions prompted us to test whether this inhibitor would also affect the transmigration of leukocytes. HUVEC monolayers were cultured on transwell filters, pretreated 48 h before the test with either control siRNA or with Tie-2 siRNA, followed 33 h later by incubation with 5 nM TNF and either 5 µM AKB-9778 or vehicle alone. The phosphatase inhibitor reduced transmigration of neutrophils by 40% (±3.9%) if the cells had been pretreated with control siRNA (Fig. 4 A). Analogous to the permeability assays in Fig. 3, inhibiting the expression of Tie-2 by siRNA increased neutrophil transmigration (Fig. 4 A), in line with a previous

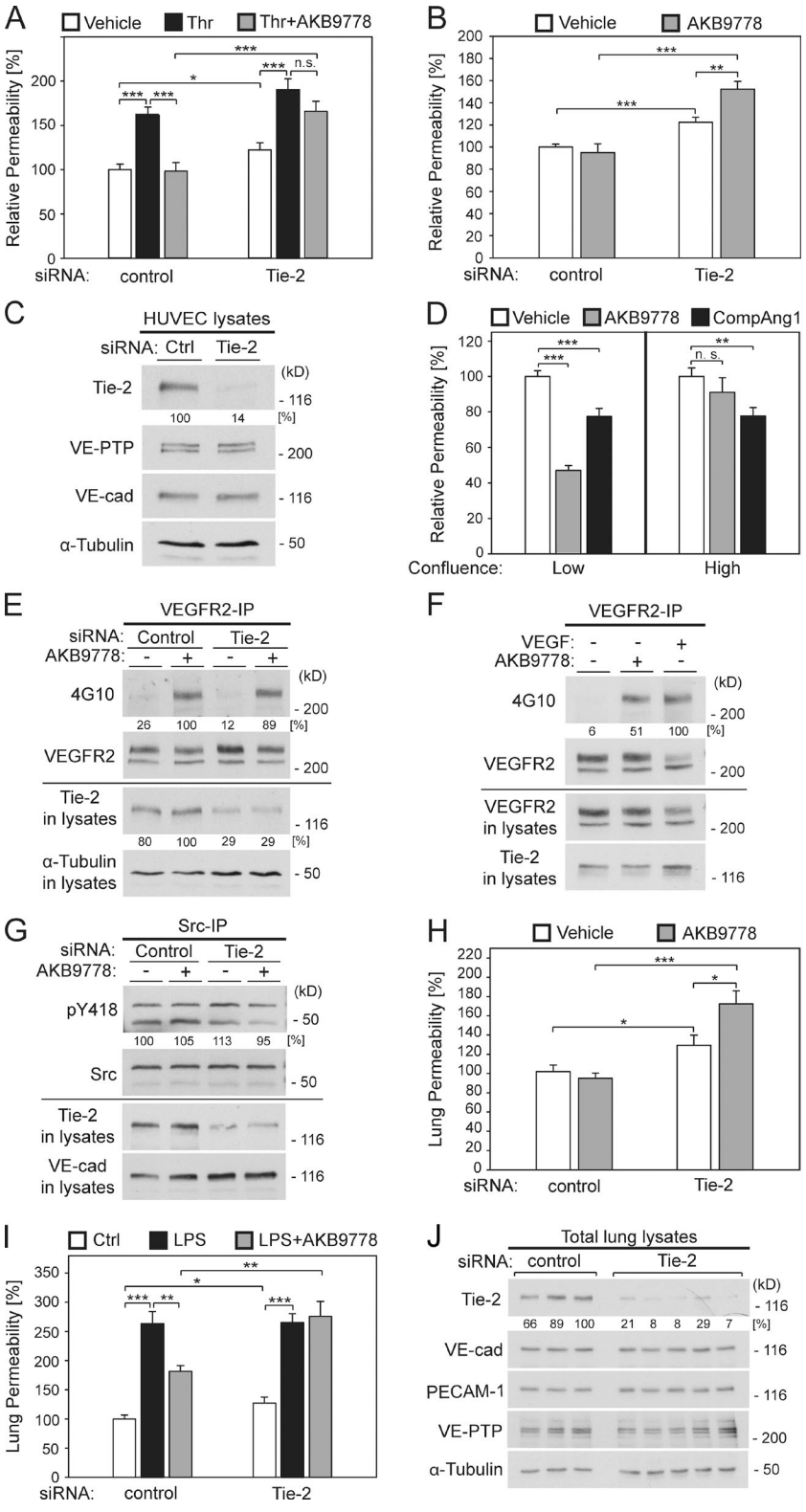

Figure 3. **Silencing of Tie-2 by siRNA eliminates the permeability-reducing effect of AKB-9778 in vitro and in vivo.** (A and B) Paracellular permeability for 250-kD FITC-dextran was determined for HUVECs transfected with control siRNA or with Tie-2–targeting siRNA (as indicated) and grown on transwell filters. (A) Cells were treated with vehicle, thrombin, or a combination of thrombin and AKB-9778 (as indicated). (B) Cells were treated with either vehicle or AKB-9778, and basal permeability was analyzed (as indicated). (C) Total cell lysates of HUVECs transfected with control siRNA or Tie-2–targeting siRNA were immunoblotted for Tie-2, VE-PTP, VE-cadherin, and α-tubulin (as indicated). (D) HUV ECs were grown on transwell filters at low (4.5×10^4 cell/cm^2) and high (1.2×10^5 cells/cm^2) confluence and treated for 30 min with 600 ng/ml Comp-Ang1, 10 µM AKB-9778, or vehicle (as indicated) before permeability for 250-kD FITC-dextran was determined under baseline conditions. Permeability of vehicle-treated cells was set to 100%. (E) VEGFR-2 was immunoprecipitated from HUVECs transfected with either control or Tie-2–targeting siRNA that were either treated with vehicle (–) or with AKB-9778 (+) for 30 min. Immunoprecipitates were immunoblotted for phospho-tyrosine (4G10) and VEGFR-2. Total lysates were immunoblotted for Tie-2 and α-tubulin (as indicated). (F) VEGFR-2 was immunoprecipitated from HUVECs that were either untreated (–) or treated with 5 µM AKB-9778 or 100 ng/ml VEGF for 30 min (as indicated). Immunoprecipitates were immunoblotted for phospho-tyrosine (4G10) and VEGFR-2 (as indicated). Total lysates were immunoblotted for VEGFR-2 and Tie-2 (as indicated). (G) Src was immunoprecipitated from HUVECs transfected with either control or Tie-2–targeting siRNA that were either treated with vehicle (–) or 5 µM AKB-9778 (+) for 30 min. Immunoprecipitates were immunoblotted for Src-pY418 and total Src. Total lysates were immunoblotted for Tie-2 and VE-cadherin (as indicated). (H) Mice were i.v. injected with either control siRNA or Tie-2–targeting siRNA (as indicated) and 48 h later subcutaneously injected with either vehicle alone or AKB-9778, followed 45 min later by i.v. injection of Evans blue. After 15 min mice were sacrificed, the lung circulation was perfused, and the dye was extracted from the lung tissue and quantified. (I) Mice were treated with control or Tie-2 siRNA as in H and then subcutaneously injected with solvent (control or LPS group) or with AKB-9778, followed by exposing them to nebulized LPS or saline (control) for 40 min. 4 h later, mice were i.v. injected with Evans blue, and 15 min later, lung permeability was measured as in H. (J) Total lung lysates of mice from H were immunoblotted for the indicated antigens. Data are pooled from four independent experiments with at least three replicates in each experiment (A and B) or two independent experiments with at least three replicates in each experiment (D) or five to six mice per group in each experiment (H–J) and representative of at least two independent experiments (C, E–G, and J). Statistical significance was analyzed using the one-way ANOVA test. *, $P \leq 0.05$; **, $P \leq 0.01$; ***, $P \leq 0.001$. Results are shown as means ± SEM.

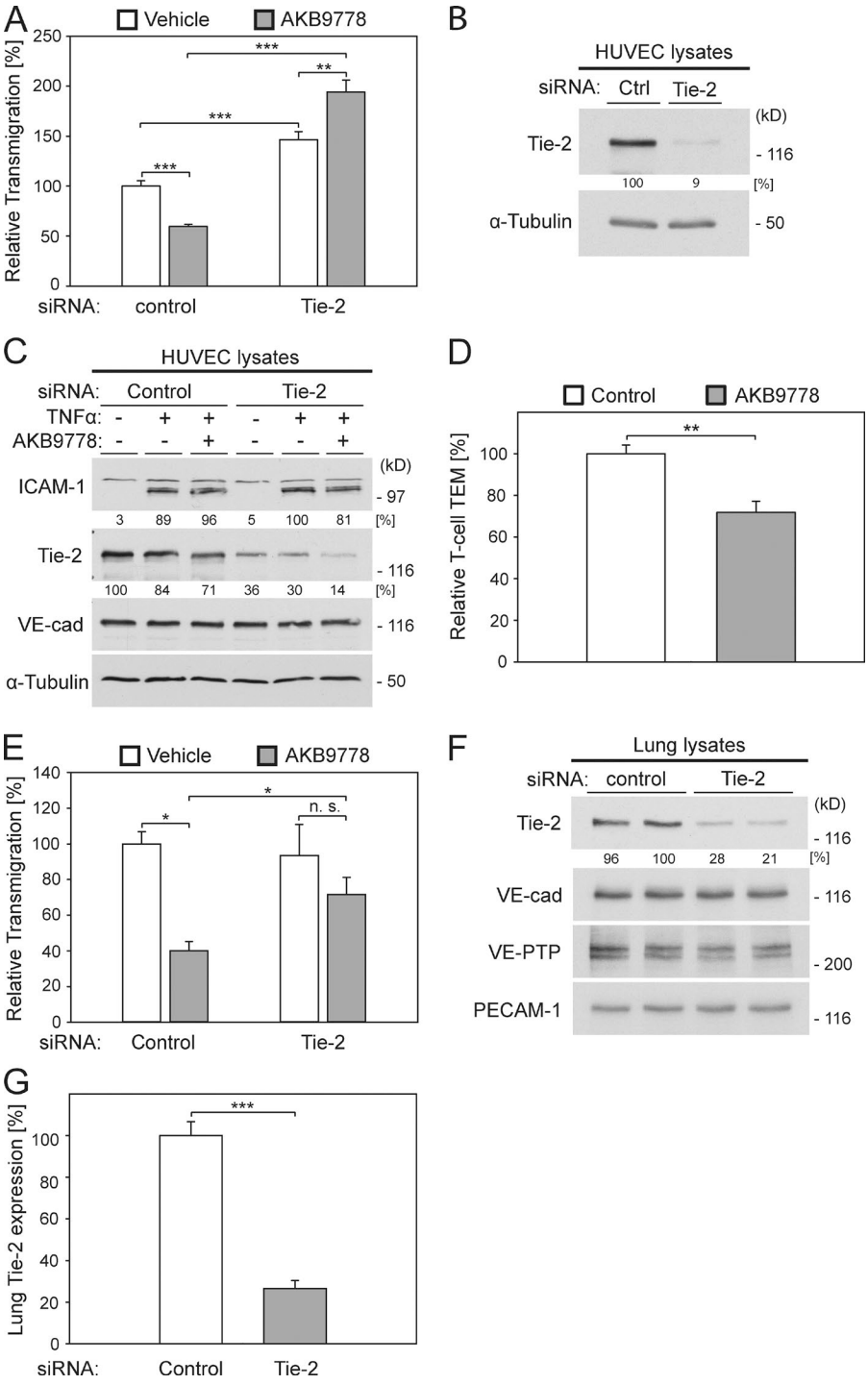

Figure 4. **Silencing of Tie-2 by siRNA eliminates the neutrophil transmigration-reducing effect of AKB-9778 in vitro and in vivo.** (A) Human neutrophils were allowed to transmigrate toward the chemokine IL-8 through a monolayer of 15-h TNF-stimulated HUVECs on transwell filters, which were either treated with 5 µM AKB-9778 or vehicle alone and transfected either with control or with Tie-2 siRNA (as indicated). The number of neutrophils that migrated across control-transfected cells was set to 100%. (B) Total cell lysates of HUVECs transfected with control siRNA or Tie-2–targeting siRNA were immunoblotted for Tie-2 and α-tubulin (as indicated). (C) HUVECs were transfected with control siRNA or Tie-2 siRNA and treated with vehicle or TNF for 18 h and in addition with vehicle or 5 µM AKB-9778 (as indicated). Total lysates were immunoblotted for ICAM-1, Tie-2, VE-cadherin, and α-Tubulin (as indicated). (D) Human T cells were allowed to transmigrate toward 100 ng/ml SDF-1α through a monolayer of HUVECs stimulated as in A with TNF and in addition with either vehicle or AKB-9778 on transwell filters. The number of T cells that migrated across vehicle-treated cells was set to 100%. (E) Mice were i.v. injected with either control siRNA or with Tie-2 siRNA (as indicated) and 48 h later subcutaneously injected with either vehicle alone or AKB-9778 (as indicated), followed 45 min later by exposing the mice to nebulized LPS for 40 min. 4 h later, mice were sacrificed, and neutrophils recruited to the alveolar space were isolated by a bronchoalveolar lavage and counted. (F) Lungs were removed from mice 48 h after i.v. injection of control siRNA or Tie-2 siRNA, and lysates were immunoblotted for the indicated antigens. (G) The mean in vivo Tie-2 knockdown efficiency of Tie-2–targeting siRNA in murine lungs was determined by quantification of Tie-2 and PECAM-1 immunoblot signals in lung lysates of mice injected with either control or Tie-2 siRNA. For quantification, 13 control siRNA– and 12 Tie-2 siRNA–injected mice were analyzed. Tie-2 signals were normalized to PECAM-1 signals and set to 100% for control siRNA–injected animals. Data are pooled from three independent experiments with three replicates in each experiment (A) or two independent experiments with six replicates in each experiment (D) or five mice per group (E and F) and representative of at least two independent experiments (B, C, and F). Statistical significance was analyzed using the one-way ANOVA test. *, $P \leq 0.05$; **, $P \leq 0.01$; ***, $P \leq 0.001$. Results are shown as means ± SEM.

study showing that Tie-2 silencing enhanced transendothelial migration of cancer cells (Hakanpaa et al., 2015). This effect was further enhanced if the VE-PTP inhibitor was added to Tie-2 siRNA–pretreated cells (Fig. 4 A). Tie-2 expression was reduced by 90% (Fig. 4 B). Neither AKB-9778 nor Tie-2 siRNA treatment affected ICAM-1 expression levels (Fig. 4 C). AKB-9778 also inhibited transmigration of human T cells through HUVECs toward stromal cell–derived factor

1α (SDF-1α; Fig. 4 D). Thus, inhibiting the activity of VE-PTP inhibits neutrophil and lymphocyte diapedesis, and this effect requires the presence of Tie-2. However, upon suppression of the expression of Tie-2, the VE-PTP inhibitor effect is reversed. Again, this junction-destabilizing effect of AKB-9778 at low levels of Tie-2 expression is in line with the supportive role of VE-PTP for the adhesive function of VE-cadherin.

Next, we tested the effect of the VE-PTP inhibitor on neutrophil recruitment into the lungs of LPS-challenged mice. AKB-9778 was injected at a single dose of 24 mg/kg subcutaneously into mice that had been treated 48 h before with ctrl siRNA. Mice inhaled aerosolized LPS for 40 min, and 4 h later neutrophils recruited into the lung were isolated by a bronchoalveolar lavage. We found that AKB-9778 inhibited neutrophil extravasation by 60% (Fig. 4 E). This inhibitory effect of AKB-9778 was strongly reduced when Tie-2 expression was suppressed by Tie-2 siRNA treatment (Fig. 4 E). Tie-2 expression was reduced by 70–80% by siRNA, as analyzed by immunoblots of lung lysates (Fig. 4, F and G). Thus, inhibition of VE-PTP attenuates leukocyte diapedesis in vitro and in vivo via Tie-2.

AKB-9778–mediated Tie-2 activation stabilizes endothelial junctions via Rap1

The opposing effects of VE-PTP inhibition on VE-cadherin function on the one hand and on junction stabilization via Tie-2 on the other hand raised the question by which mechanism AKB-9778 enhances junction stability. It has been suggested that Tie-2 activation stabilizes junctions via stimulating Rac1, which causes deactivation of RhoA (Mammoto et al., 2007). In line with this, we found that both 10 μM AKB-9778 and 200 ng/ml Comp-Ang1 activate the GTPase Rac1 in HUVECs (Fig. 5 A).

Next we tested whether AKB-9778 would reverse the activating effect of thrombin on the phosphorylation of nonmuscle myosin light chain (MLC). As shown in Fig. 5 B, incubation of HUVECs for 2 min with 1 U/ml thrombin enhanced phosphorylation of MLC at Thr18 and Ser19, as was detected in immunoblots. This effect was clearly reduced by AKB-9778 (Fig. 5 B).

In agreement with these effects, we found that thrombin-enhanced formation of radial stress fibers in monolayers of HUVECs was reduced by AKB-9778, as was shown by F-actin staining (Fig. 5 C). Linearization of junctions by AKB-9778, as visualized by staining for VE-cadherin, pointed toward reduced mechanical tension on cell contacts (Fig. 5 C).

To identify signaling steps that would be triggered by VE-PTP inhibition upstream of the activation of Rac1, we tested for the activation of Rap1, a GTPase that is well known to stabilize EC junctions. We found that incubation of HUVECs for 10 min with 10 μM AKB-9778 strongly enhanced the activation of Rap1 (Fig. 5 D). Knocking down Rap1A and Rap1B simultaneously blocked the stimulatory effect of AKB-9778 on Rac1 activation (Fig. 5 E). In addition, siRNA for Rap1A and Rap1B also blocked the stabilizing effect of AKB-9778 on the barrier function of HUVEC monolayers challenged by thrombin and determined in permeability assays (Fig. 5 F). Rap1 expression was reduced by 88% by siRNA, as analyzed by immunoblots of HUVEC lysates (Fig. 5 G). Thus, AKB-9778 stimulates Rac1 and stabilizes EC contacts via Rap1.

Tie-2 activation by multimeric Ang1 was recently found to induce rapid redistribution of Tie-2 to the EC contacts (Fukuhara et al., 2008; Saharinen et al., 2008). It is an attractive hypothesis that this redistribution might be involved in the cell contact–stabilizing effect. To test this, we asked whether AKB-9778 would also induce the redistribution of Tie-2 to cell contacts. We found that 600 ng/ml Comp-Ang1 induced a strong accumulation of Tie-2 at cell contacts in fully confluent as well as in less confluent HUVEC monolayers; however, 5 μM AKB-9778 had no such effect (Fig. 6, A and B). As controls, we found that 5 μM AKB-9778 and 200 ng/ml and 1 μg/ml Comp-Ang1 induced Tie-2 tyrosine phosphorylation (Fig. 6 C). In line with this, both AKB-9778 and Comp-Ang1 efficiently reduced thrombin-induced permeability of HUVEC monolayers for 250-kD FITC-dextran (Fig. 6 D).

Collectively, we conclude that inhibition of VE-PTP stabilizes endothelial junctions via activation of Rap1, which acts upstream of Rac1 activation, and leads to reduced nonmuscle MLC phosphorylation and radial stress fiber formation. In addition, making use of this indirect way of Tie-2 activation allowed us to show that stabilization of EC contacts by stimulating Tie-2 kinase activity does not require an increase or accumulation of Tie-2 molecules at EC junctions. However, this does not rule out that it is Tie-2 at cell contacts, which mediates contact strengthening via Ang-1.

Analysis of endothelial junction integrity in conditional *Cdh5*$^{lox/lox}$ gene–deficient mice

To test the relevance of VE-cadherin for the VE-PTP/Tie-2–induced stabilization of EC contacts, we generated conditional *Cdh5* gene–deficient mice by flanking exon 2 (containing the start codon) with loxP sites (Fig. 7, A and B). Homozygous *Cdh5*$^{lox/lox}$ mice expressing tamoxifen-inducible *Cdh5-iCre* (*Cdh5*^{iECKO}) or no *Cre* were stimulated at the age of 7 wk with tamoxifen daily for five consecutive days; 2 d later, Evans blue was injected i.v. for 30 min, and extravasated dye was determined in skin, heart, lung, and the brain. We found that inactivation of *Cdh5* caused massive extravasation of the dye in lung and heart, whereas no leaks were observed in skin and brain (Fig. 7 C). Ablation of *Cdh5* led to an almost complete loss of VE-cadherin protein in brain, lung, heart, and skin, as was analyzed by immunoblotting tissue lysates (Fig. 7, D and E). There was no difference in claudin-5 expression detectable in brains of WT and *Cdh5*^{iECKO} mice, as confirmed by immunoblotting of brain lysates (Fig. 7 D).

Despite the dramatic increase of vascular permeability in the lung of *Cdh5*^{iECKO} mice, endothelial junctions in capillaries, venules, and arterioles appeared intact when analyzed by electron microscopy. No obvious differences were found

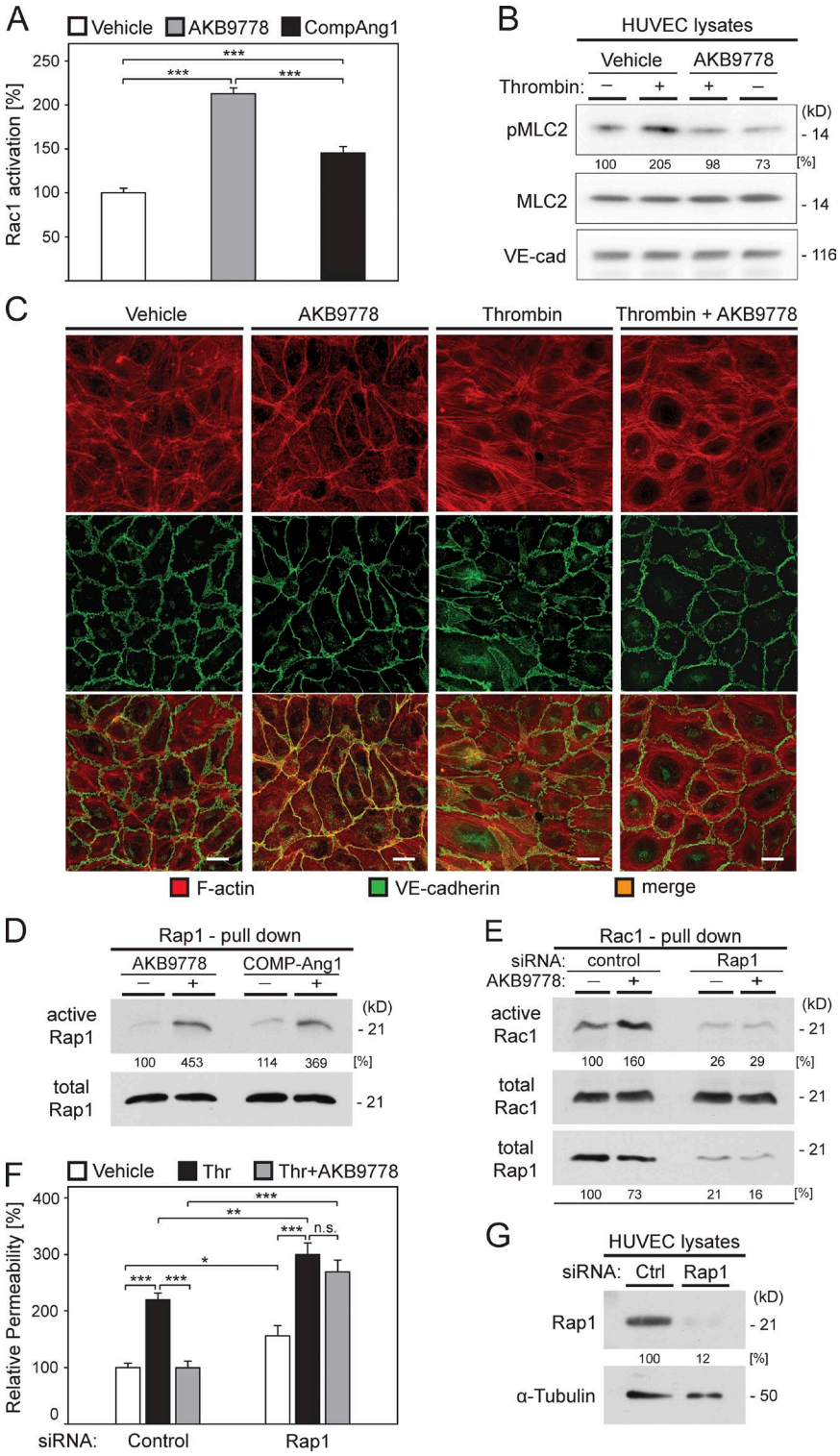

Figure 5. **AKB-9778–triggered stimulation of Tie-2 stabilizes EC contacts via activation of Rap1.** (A) HUVECs were treated for 30 min with AKB-9778, COMP-Ang1, or vehicle (as indicated), followed by analyzing the activation level of Rac1 by a luminescence-based G-LISA Rac1 activation assay. (B) HUVECs were either pretreated with solvent (vehicle) or with AKB-9778 for 30 min before solvent (–) or thrombin (+) was added and incubated for 2 min (as indicated), followed by immunoblotting cell lysates for phospho-Thr18/Ser19 of nonmuscle MLC (pMLC2), MLC2, and VE-cadherin. (C) Confluent HUVEC monolayers were treated with either solvent (vehicle) or AKB-9778 for 30 min before thrombin was added and incubated (as indicated) for 15 min, followed by staining of fixed and permeabilized cells for F-actin and VE-cadherin. Bars, 20 µm. (D) HUVECs were either left untreated (–) or treated with AKB-9778 or with COMP-Ang1, followed by a pull-down assay for Rap1 and immunoblotting for this GTPase. (E) HUV ECs were transfected with control siRNA or Rap1 siRNA. 72 h later, cells were treated with 10 µM AKB-9778 for 10 min, and Rac1 activity was measured by a pull-down experiment with the effector protein PAK, and active Rac1 was compared with total levels of Rac1. Total levels of Rap1 are shown at the bottom. (F) HUVECs were silenced for Rap1 as in E, grown on transwell filters, and treated for 30 min with thrombin either in the presence of solvent (vehicle) or of AKB-9778 (as indicated). Permeability for 250-kD FITC-dextran was determined as for Fig. 1. (G) Total cell lysates of HUVECs transfected with control siRNA or Rap1-targeting siRNA were immunoblotted for Rap1 and α-tubulin (as indicated). Data are pooled from three independent experiments with three replicates in each experiment (A) or at least two independent experiments (B–G). Statistical significance was analyzed using the one-way ANOVA test. *, $P \leq 0.05$; **, $P \leq 0.01$; ***, $P \leq 0.001$. Results are shown as means ± SEM.

between vessels in skin, heart, lung, and brain (Fig. 8 A). Likewise, the mean length of junctions was not affected by *Cdh5* gene inactivation (Fig. 8 C). Thus, the leakiness for plasma protein–adsorbed Evans blue was not accompanied by ultrastructural defects of junctions. Furthermore, histological analysis of sections of paraffin-embedded lungs did not reveal obvious vascular abnormalities or signs of bleeding (Fig. 8 B).

Because it was reported that loss of VE-cadherin leads to its replacement by N-cadherin in endothelial junctions (Giampietro et al., 2012), we tested whether this would be

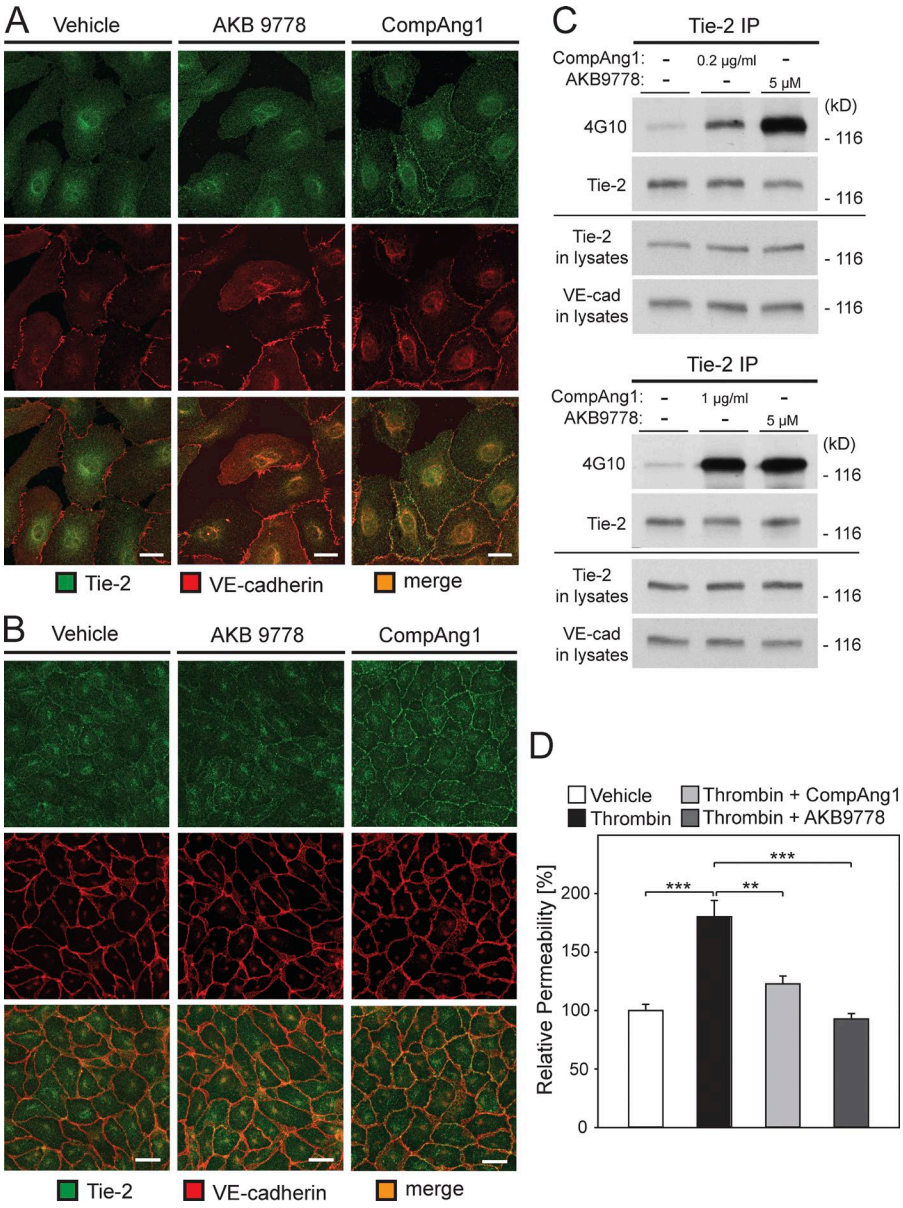

Figure 6. **COMP-Ang1 and AKB-9778 both stimulate tyrosine phosphorylation of Tie-2, but only Comp-Ang1 redistributes Tie-2 to EC contacts.** HUVECs were grown at low confluence (1.5×10^4 cells/cm^2; A) and at high confluence (7×10^4 cells/cm^2; B) and treated with solvent (vehicle), 5 µM AKB-9778, or 600 ng/ml COMP-Ang1 for 30 min, followed by fixation, permeabilization, and staining for Tie-2 and VE-cadherin. Bars, 20 µm. (C) Immunoprecipitates of Tie-2 from cell lysates of HUVECs treated with reagents as indicated were immunoblotted for phospho-tyrosine (4G10) and Tie-2. (D) HUVECs were treated with solvent (vehicle), AKB-9778, or COMP-Ang1 for 30 min before thrombin was added (as indicated), and permeability for 250-kD FITC-dextran was determined. Data are representative of at least two independent experiments (A and B) and pooled from two independent experiments with three replicates in each experiment (C). Statistical significance was analyzed using the one-way ANOVA test, and for D the Mann-Whitney rank sum test was used. **, $P \leq 0.01$; ***, $P \leq 0.001$. Results are shown as means ± SEM.

the reason for the stability of endothelial junctions in the skin. Indeed, N-cadherin was up-regulated upon tamoxifen treatment of skin-derived primary ECs of *Cdh5*^{iECKO} mice (Fig. 9 A), and N-cadherin replaced VE-cadherin at junctions (Fig. 9 B). However, in vivo inactivation of *Cdh5*, confirmed by whole mount stainings (Fig. 9 C) and immunoblots of the skin (Fig. 7 E), did not lead to the replacement of VE-cadherin by N-cadherin at endothelial junctions of blood vessels of the skin, as shown in whole mount stainings (Fig. 9 D). Nonjunctional, patchy staining of some vessels for N-cadherin was at the basal surface of ECs, colocalized with the perivascular cell marker NG2, and was seen independent of *Cdh5* inactivation (Fig. 9 E). Remarkably, even β-catenin staining was not detected anymore at EC contacts of skin blood vessels upon inactivation of *Cdh5* (Fig. 9 F). In combination with our electron microscopy analysis, this surprising finding suggests that endothelial junctions, once they are formed in adult vessels, can maintain their structure even in the absence of cadherins.

VE-PTP inhibition stabilizes endothelial junctions in the absence of VE-cadherin

Because VE-cadherin is required for the stability of endothelial junctions in the lung, we tested whether the Tie-2–mediated stabilizing effect of the VE-PTP inhibitor on vessel integrity in the lung would require VE-cadherin. *Cdh5*^{iECKO} mice, and for controls *Cdh5*$^{lox/lox}$ mice without the *Cre* transgene, were treated with tamoxifen as described in the previous section and exposed to aerosolized LPS for 40 min, and vascular permeability was determined by injecting Evans blue

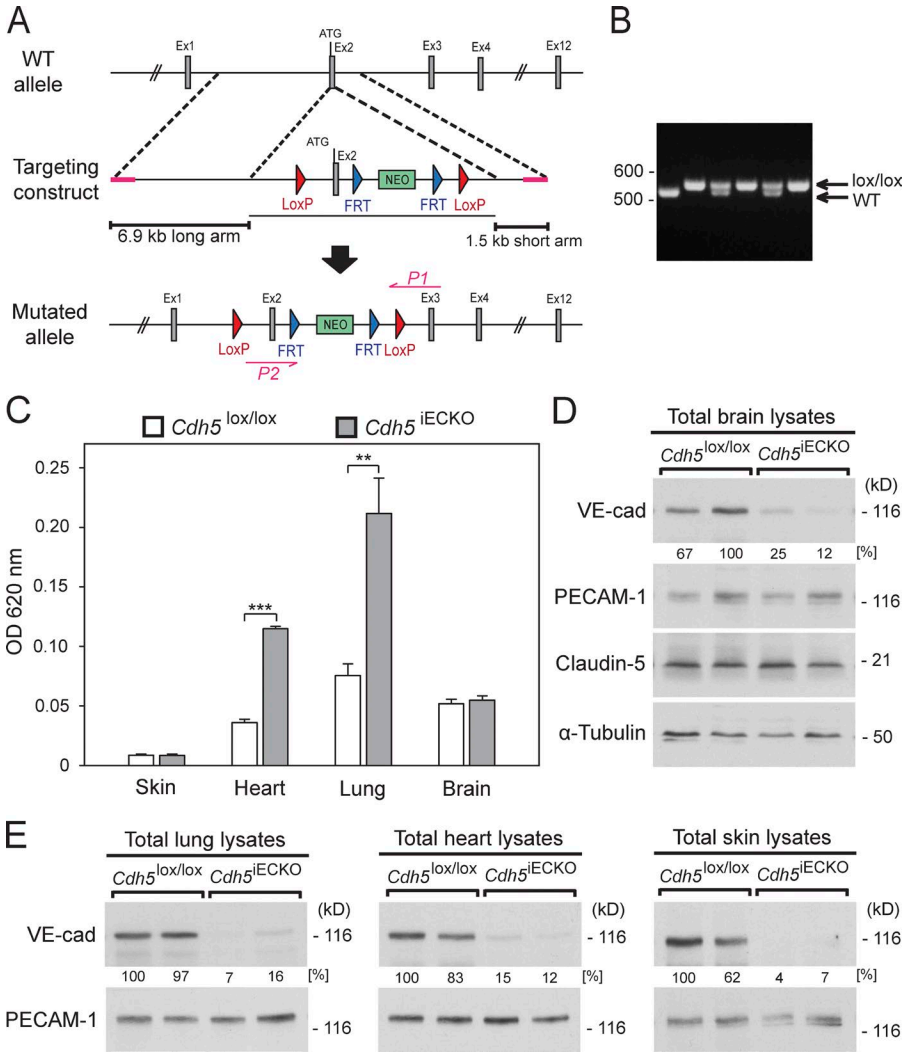

Figure 7. **Conditional *Cdh5* gene inactivation in mice and analysis of its effect on vascular permeability.** (A) A map of the relevant genomic region is shown, with ATG-containing exon 2, flanked by loxP sites. P1 and P2 represent oligonucleotides used for PCR screening. (B) PCR genotyping using primers P1 and P2 resulted in 565-bp or 520-bp products for the mutant or WT allele, respectively. (C) $Cdh5^{lox/lox}$ or $Cdh5^{iECKO}$ mice were i.p. injected with tamoxifen daily for 5 d. 2 d later, Evans blue was i.v. injected, mice were sacrificed after 30 min, the body circulation was perfused, and the dye was extracted from samples of various organs (as indicated) and quantified. (D and E) Lysates of tissue samples from brain (D) and lung, heart, and skin (E) of tamoxifen-treated $Cdh5^{lox/lox}$ and $Cdh5^{iECKO}$ mice were immunoblotted for the indicated antigens. Data are pooled from at least two independent experiments with five to six mice per group in each experiment (C and D). Statistical significance was analyzed using the one-way ANOVA test. **, $P \leq 0.01$; ***, $P \leq 0.001$. Results are shown as means ± SEM.

4 h later for 5 min. As shown in Fig. 10 A, inactivation of *Cdh5* increased lung vascular permeability, and exposure to LPS augmented the extravasation of Evans blue even further. Administration of AKB-9778 compensated the LPS-induced increase of vascular permeability in $Cdh5^{iECKO}$ mice. Gene inactivation resulted in a reduction of VE-cadherin to hardly detectable amounts, as determined by immunoblotting lung lysates for VE-cadherin (Fig. 10 C). Thus, blocking of inflammation-induced vascular permeability by the VE-PTP inhibitor AKB-9778 does not require VE-cadherin. Interestingly, the lack of VE-cadherin could not be compensated by AKB-9778. In agreement with this, we could also not block the permeability-increasing effect of i.v. injected anti–VE-cadherin mAb BV13 by AKB-9778 (Fig. 10 B).

Next we tested whether inflammation-induced leukocyte extravasation would be enhanced by *Cdh5* gene ablation and whether activation of Tie-2 by inhibition of VE-PTP could counteract this effect. $Cdh5^{iECKO}$ mice, and for control $Cdh5^{lox/lox}$ mice, were treated with tamoxifen as described in the previous section and exposed to aerosolized LPS for 40 min, and 4 h later, neutrophils recruited into the lungs were removed by bronchoalveolar lavage and counted. We found that inactivation of *Cdh5* did indeed enhance neutrophil extravasation (Fig. 10 D). AKB-9778 attenuated LPS-induced neutrophil extravasation in mice no matter whether they expressed VE-cadherin or not. Again, AKB-9778–triggered Tie-2–mediated stabilization of endothelial junctions does not require VE-cadherin, and this inhibits neutrophil recruitment into the inflamed lung.

We showed that the junction-stabilizing effect of AKB-9778 is based on Tie-2–driven activation of Rap-1, which in turn activates Rap-1 (Fig. 5). To test whether these effects are indeed independent of VE-cadherin, we isolated lung ECs from $Cdh5^{iECKO}$ mice and treated them in culture for 54 h either with 4-hydroxytamoxifen or solvent alone, followed by a pull-down assay for Rap-1 or Rac-1. As shown in Fig. 10 (E and F), activation of both GTPases by AKB-9778 was seen independent of the presence of VE-cadherin. Efficiency of *Cdh5* inactivation was demonstrated by immunoblotting cell lysates for VE-cadherin.

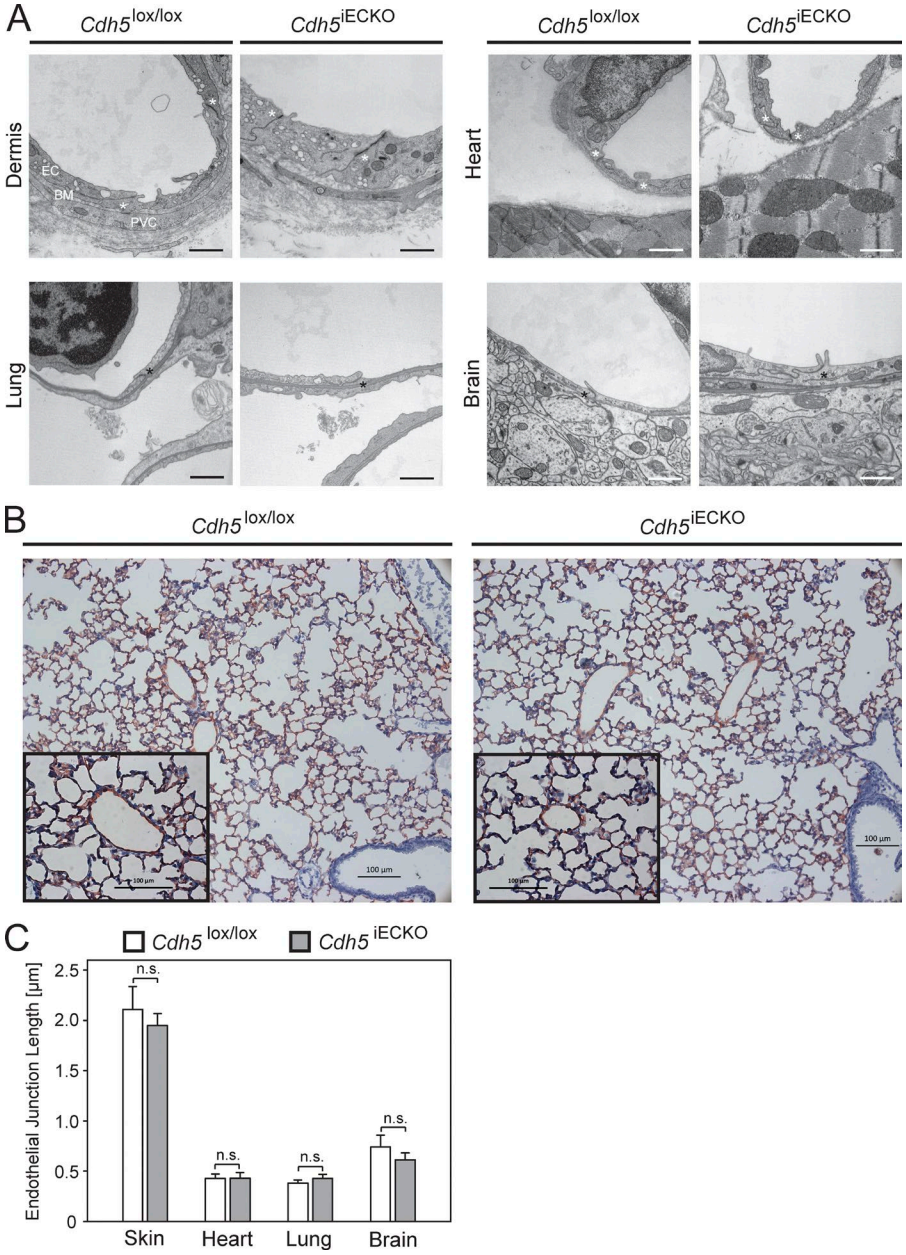

Figure 8. **Endothelial Junctions of *Cdh5*^{iECKO} mice appear largely normal in lung, heart, skin, and brain, and lungs show no obvious vascular malformation or hemorrhage.** (A) Electron microscopy of endothelial junctions in skin, heart, lung, and brain of tamoxifen-treated *Cdh5*^{iECKO} mice. Note that junctions (asterisks) appeared largely normal. BM, basement membrane; PVC, perivascular cells. (B) Paraffin sections of the lung of tamoxifen-treated *Cdh5*$^{lox/lox}$ mice and *Cdh5*^{iECKO} mice were stained for the endothelial marker endomucin. Insets show representative sections at a three-times-higher magnification. No signs of bleeding or tissue damage were observed. Bars: (A) 1 µm; (B) 100 µm. (C) The mean length of endothelial junctions was determined in electron microscopy pictures of skin, heart, lung, and brain in tamoxifen-treated *Cdh5*$^{lox/lox}$ and *Cdh5*^{iECKO} mice using the software Fiji. For the quantification, 86 junctions in the skin, 15 junctions in the heart, 51 junctions in the lung, and 41 junctions in the brain were analyzed. Data are representative of at least two independent experiments with at least three mice per group in each experiment (A) and two independent experiments with at least two mice in each experiment (B). Statistical significance was analyzed using the one-way ANOVA test. Results are shown as means ± SEM.

DISCUSSION

In this study, we report on the dual role of VE-PTP for the regulation of endothelial junctions and the consequences for vascular permeability and leukocyte extravasation in vivo. Disruption of VE-PTP activity by genetic ablation or pharmacologic inhibition with extracellular domain antibodies or the selective phosphatase inhibitor AKB-9778 protected against the induction of vascular permeability by various inflammatory mediators. In addition, inhibition of VE-PTP also blocked neutrophil recruitment into the lungs of LPS-challenged mice. Targeting the expression of Tie-2 enabled us to demonstrate the following: first, that Tie-2 is responsible for the protective effect of VE-PTP inhibition on vessel integrity; second, that Tie-2 expression is required to maintain baseline integrity of the vessel wall; and third, that the absence of Tie-2 enables VE-PTP inhibition to destabilize endothelial junctions, which highlights the supportive effect of VE-PTP for the adhesive function of VE-cadherin in vivo. Surprisingly, our results demonstrate that the stabilizing effect of AKB-9778 on junctions via Tie-2 overrides the destabilizing effect caused by inhibiting VE-cadherin–mediated adhesion. Moreover, and in line with this, AKB-9778 could even stabilize endothelial junctions and vessel integrity in the absence of VE-cadherin. This junction-stabilizing effect of AKB-9778 is based on Tie-2–driven activation of Rap1, which in turn activates Rac1 and leads to the dissolution of radial stress fibers.

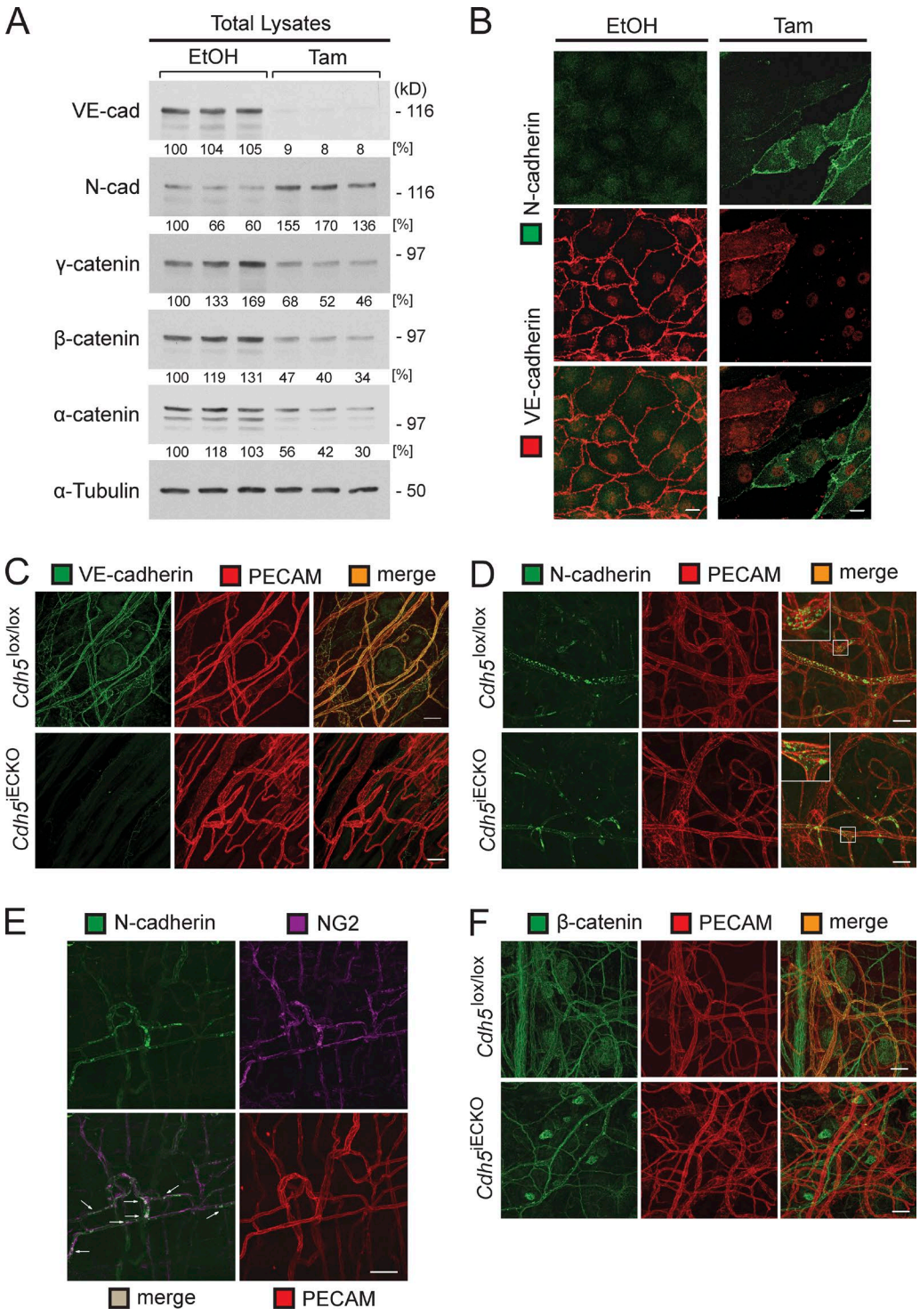

Figure 9. **VE-cadherin is replaced by N-cadherin in cultured ECs of *Cdh5*^{iECKO} but not by N-cadherin or other cadherins in blood vessels of the skin.** (A) ECs were isolated from the skin of *Cdh5*^{iECKO} mice and treated with solvent (EtOH) or 4-hydroxytamoxifen (Tam), and cell lysates were immunoblotted for the indicated antigens. (B) ECs isolated from the skin of *Cdh5*^{iECKO} mice were treated with solvent (EtOH) or 4-hydroxytamoxifen and stained for the indicated antigens. (C and D) Whole mount stainings of the skin of *Cdh5*$^{lox/lox}$ and *Cdh5*^{iECKO} mice for the indicated antigens. Insets in D show the indicated sector at a three-times-higher magnification. (E) Whole mount stainings of the skin of WT mice stained for N-cadherin and the pericyte marker NG2. Arrows mark white areas indicating NG2/N-cadherin colocalization. (F) Whole mount stainings of the skin of *Cdh5*$^{lox/lox}$ and *Cdh5*^{iECKO} mice for the indicated antigens. Data are representative of at least two independent experiments (A–F) with at least three mice per group in each experiment (C–F). Bars: (B) 20 µm; (C–F) 50 µm.

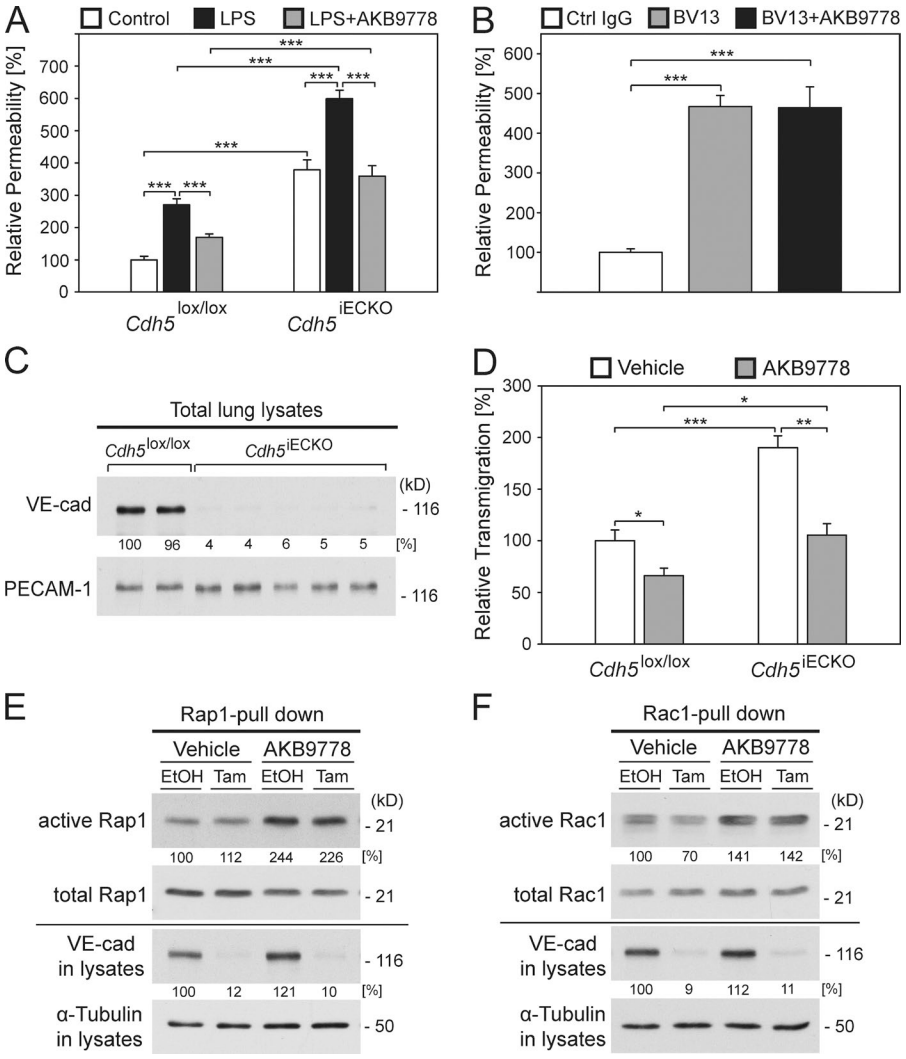

Figure 10. **AKB-9778 counteracts LPS-induced leakiness and neutrophil recruitment in the lung even in the absence of VE-cadherin.** (A) *Cdh5*$^{lox/lox}$ or *Cdh5*^{iECKO} mice were i.p. injected with tamoxifen daily for 5 d and, 2 d later, subcutaneously injected with solvent (ctrl or LPS group) or with AKB-9778 and then exposed to nebulized LPS or saline (ctrl) for 40 min. 4 h later, mice were i.v. injected with Evans blue and 5 min later sacrificed; the lung circulation was perfused, and the dye was extracted from the lung tissue and quantified. (B) Mice were subcutaneously injected with either vehicle alone or AKB-9778 and 30 min later i.v. injected with either 60 µg/mouse control IgG or BV13 (as indicated). 2 h later, Evans blue was i.v. injected. After 15 min, mice were sacrificed, the lung circulation was perfused, and the dye was extracted from the lung tissue and quantified. (C) Total lung lysates of mice from D were immunoblotted for the indicated antigens. (D) *Cdh5*$^{lox/lox}$ or *Cdh5*^{iECKO} mice were treated with tamoxifen and LPS as in A, and extravasated neutrophils were isolated by bronchoalveolar lavage and counted. (E and F) ECs were isolated from the lungs of *Cdh5*^{iECKO} mice, treated in culture for 54 h with solvent (EtOH) or 4-hydroxytamoxifen (Tam), and stimulated for 30 min either with vehicle or AKB-9778 (as indicated), followed by a pull-down assay for Rap1 (E) or Rac1 (F) and immunoblotting for the analyzed GTPase. Total cell lysates were immunoblotted for VE-cadherin and α-tubulin (as indicated). Data are pooled from two independent experiments with four mice per group in each experiment (A) or two to three mice per group in each experiment (B) or five mice per group in each experiment (D) and representative of at least two independent experiments (C, E, and F). Statistical significance was analyzed using the one-way ANOVA test. *, $P \leq 0.05$; **, $P \leq 0.01$; ***, $P \leq 0.001$. Results are shown as means ± SEM.

Although AKB-9778 is a highly specific inhibitor of the catalytic activity of VE-PTP (Shen et al., 2014), the present study is the first to demonstrate that this inhibitor stabilizes vessel integrity indeed via VE-PTP and that the substrate responsible for this effect is Tie-2. The essential role of VE-PTP for the junction-stabilizing effect of AKB-9778 was demonstrated because this effect of the inhibitor was no longer observed in *Ptprb*^{iECKO} mice. The question of which VE-PTP substrate would be responsible for the junction-stabilizing effect is important in light of other substrates that have been described. Besides VE-cadherin and Tie-2, VE-PTP had been reported to interact with and to affect the activity of the VEGFR-2, an interaction that was suggested to be relevant for endothelial sprouting (Mellberg et al., 2009; Hayashi et al., 2013). Furthermore, other tyrosine kinase receptors were described as possible substrates based on binding to a phosphatase-trapping mutant (Sakuraba et al., 2013). In this context, it is important that expression of Tie-2 was indeed required for the AKB-9778–stabilizing effect on endothelial junctions.

Several substrates of VE-PTP are likely to be involved in the junction-destabilizing effect of AKB-9778 under conditions of low or no Tie-2 expression. These are VE-cadherin itself and plakoglobin (Nottebaum et al., 2008; Wessel et al., 2014) and VEGFR-2 (Hayashi et al., 2013), which are involved in the regulation of junctions. Whether other potential substrates of VE-PTP (Sakuraba et al., 2013) are relevant for the stabilizing effect of VE-PTP on endothelial junctions is at present unknown.

Stimulation of Tie-2 by Ang-1 protects the vasculature against plasma leaks (Gamble et al., 2000; Thurston et al., 2000). Various signaling mechanisms were suggested to mediate this effect. Ang-1 was shown to trigger the activation

of RhoA, which caused the sequestration of Src by mDia, and thereby inhibition of VEGF-induced VE-cadherin phosphorylation and endocytosis (Gavard et al., 2008). In line with this, it was reported that Ang1 triggers the recruitment of the RhoA-specific GEF Syx to endothelial junctions, which supported RhoA-mediated activation of mDia (Ngok et al., 2012). Others reported that stimulation of Tie-2 leads to the activation of Rac1, which triggered via p190RhoGAP the deactivation of RhoA, which in turn blocked rearrangements of the actin cytoskeleton caused by inflammatory mediators (Mammoto et al., 2007; David et al., 2011). Our results are in line with the latter studies. AKB-9778–mediated stimulation of Tie-2 activated Rac1 and dissolved the formation of actomyosin-based radial stress fibers, releasing the tension on endothelial junctions. With the activation of Rap1, we have identified an essential step upstream of Rac1, via which Tie-2 stabilizes endothelial junctions. In addition to Rac-1, Rap-1 could also more directly modulate the activity of RhoA via the RhoGAP ArhGAP29 (Post et al., 2013).

Rap1 activation, although hitherto unknown as a signaling target of Tie-2, is well established as a signaling step that leads to the reinforcement of endothelial junctions. This is achieved by two "parallel" pathways, the dissolution of radial stress fibers via suppression of the Rho–Rock–nonmuscle myosin II pathway, and by the formation of circumferential actin bundles via activation of Cdc42 (Ando et al., 2013). Both of these effects on radial stress fibers and circumferential actin filaments were observed with AKB-9778 in HUVECs (Fig. 5). It is reasonable to assume that these effects would enhance the adhesive activity of VE-cadherin, and it has indeed been demonstrated very convincingly that activation of Rap1 reinforces VE-cadherin–mediated endothelial junction integrity (Fukuhara et al., 2005; Kooistra et al., 2005; Mochizuki, 2009). Remarkably, however, our results indicate that the Tie-2/Rap1-mediated effects on the actomyosin cytoskeleton are even able to reinforce endothelial junctions in the absence of VE-cadherin. Our results do not argue against mechanisms whereby Tie-2/Rap1 signaling enhances VE-cadherin–mediated adhesion, but they suggest that this signaling pathway is not essential to stabilize endothelial junctions via Tie-2 stimulation in vivo.

It has been demonstrated that Ang1 triggers the redistribution of Tie-2 together with VE-PTP to endothelial junctions in endothelial monolayers, whereas scattered mobile ECs accumulate Tie-2 at cell matrix contacts (Fukuhara et al., 2008; Saharinen et al., 2008). These studies established that distinct Tie-2 signaling complexes were recruited to different sites in quiescent and mobile cells. This explained how Tie-2 manages to stimulate different signaling pathways in vascular quiescence and angiogenesis. Our results demonstrate that the redistribution of Tie-2 to cell contacts is not automatically triggered by activation of Tie-2 kinase activity, but requires the binding of Ang-1.

The fact that stimulation of Tie-2 by the VE-PTP inhibitor AKB-9778 stabilizes challenged endothelial junctions even in the absence of VE-cadherin is noteworthy for at least two reasons. First, this explains why the negative effect of AKB-9778 on the adhesive function of VE-PTP–associated VE-cadherin does not jeopardize the ability of AKB-9778 to reinforce junction integrity via Tie-2. Second, our results suggest that inflammation-induced opening of endothelial junctions is a two-step mechanism. It does require reduction of the adhesive function of VE-cadherin, as has been shown before with mutant knock-in mice expressing either a VE-cadherin–α-catenin fusion protein or VE-cadherin tyrosine mutants replacing endogenous VE-cadherin (Schulte et al., 2011; Wessel et al., 2014). In addition to the weakening of the adhesive integrity of endothelial junctions and independent of this, inflammatory stimuli open endothelial junctions via enhancing actomyosin-mediated pulling forces on cell contacts. AKB-9778–induced Tie-2 activation can abrogate this effect. It was unexpected that inflammation-induced effects on the actomyosin cytoskeleton further enhanced the opening of endothelial junctions even in the absence of VE-cadherin. Likewise, it is interesting that dampening the formation of radial stress fibers via Rap1 activation could still stabilize challenged endothelial junctions even when VE-cadherin was absent.

VE-cadherin is very well established as an adhesion molecule of dominant importance for the formation and the stability of endothelial junctions (Dejana and Vestweber, 2013). Therefore, we were surprised to observe no leak formation in skin and brain despite efficient *Cdh5* gene inactivation even at 7 d after the onset of Cre expression. In line with this, antibodies against VE-cadherin enhanced vascular permeability in lung and heart within hours but had no effect in skin and brain (Corada et al., 1999). However, lack of antibody-induced leak formation in skin and brain could have been caused by an insufficient accessibility of VE-cadherin for the antibodies. The present results circumvent this limitation. We can, however, not fully exclude that low-level leakage of plasma content might occur over longer time periods. In fact, at 17–20 d after onset of Cre expression, we detected edema formation in the dermis (unpublished data). This could either be caused by subtle junctional defects or by insufficient heart function.

Cdh5 gene–inactivated mice survived for at least 20 d. This demonstrates that tight junctions of the blood–brain barrier (BBB) were not dramatically affected and that maintenance of BBB integrity does not require VE-cadherin. For comparison, $Cldn5^{-/-}$ mice die within 10 h after birth as the result of a defective BBB (Nitta et al., 2003). In agreement with this, we detected normal levels of claudin-5 in brain lysates of $Cdh5^{iECKO}$ mice at day 7 after onset of Cre expression. Because absence of VE-cadherin was reported to cause a loss of claudin-5 expression in cultured ECs and in fragments of endothelial clusters that formed in allantois explant cultures of $Cdh5^{-/-}$ mice (Taddei et al., 2008), we assume that VE-cadherin is relevant for the expression of claudin-5 in newly forming vessels that establish cell contacts, whereas

fully established blood vessels do not need VE-cadherin to maintain claudin-5 expression and tight junction integrity.

We did not detect any obvious defects of endothelial junctions in *Cdh5*^{iECKO} mice by ultrastructural analysis of vessel sections in skin and brain. Even lung and heart endothelial junctions looked largely normal, despite the enhanced leakiness for plasma proteins. We can exclude that another cadherin was compensating the loss of VE-cadherin in skin blood vessels because we could neither detect N-cadherin nor β-catenin at endothelial junctions in skin whole mounts. In contrast, in vitro we found that N-cadherin was up-regulated in cultured primary ECs upon inactivation of *Cdh5* and was found at junctions, in line with a previous study (Giampietro et al., 2012). We conclude that in vivo the loss of VE-cadherin in fully established blood vessels in the adult skin is not compensated by other cadherins. Thus, it is remarkable that endothelial adherens junctions in established blood vessels in skin and brain can be maintained in the absence of cadherins. Furthermore, enhanced basal permeability for plasma proteins in lung and heart caused by the absence of VE-cadherin is not accompanied with the complete destruction of junctions, but rather with a more subtle destabilization that does not correspond with damage that would be detectable by electron microscopy.

In conclusion, our results highlight the significance and interrelationship of VE-cadherin, Tie-2, and VE-PTP as regulators of endothelial junctions and vessel integrity in vivo. We show that inhibition of VE-PTP, although blocking its support for associated VE-cadherin, strengthens junction integrity via Tie-2. This latter effect relies on Rap1 that stimulates the dissolution of radial stress fibers and can support junction strengthening even in the absence of VE-cadherin. Our results suggest that inflammation-induced weakening of endothelial junctions is a two-step process that requires targeting of VE-cadherin and/or associated proteins (Schulte et al., 2011; Wessel et al., 2014) plus interference with the actomyosin system. The latter of these effects is dampened by activation of Tie-2. Targeting of VE-cadherin is necessary but not always sufficient for opening of endothelial junctions in vivo because VE-cadherin gene inactivation had only dramatic effects on junction stability in organs exposed to strong mechanic challenge, such as lung and heart. Especially the stability of the BBB several weeks after VE-cadherin gene inactivation was surprising. This unexpected stability of endothelial junctions in the absence of VE-cadherin may be explained by stability-enforcing structures such as the basement membrane and perivascular cells in established adult blood vessels. Furthermore, other adhesion molecules might be relevant for the stability of endothelial junctions, in addition to VE-cadherin. Revealing their identity will be an interesting goal for the future.

MATERIALS AND METHODS

Cell culture and reagents. HUVECs were cultured in EBM-2 medium supplemented with SingleQuots (Lonza). Primary ECs from lung of WT or gene-inactivated mice were isolated and cultured as previously described (Schulte et al., 2011). For isolation of ECs from skin, tails were cut at the base and transferred into sterile HBSS/1% Pen/Strep before the skin was removed from the tails and cut into 20-mm-long fragments. The fragments were incubated in 5% Dispase/PBS for 60 min at 37°C with gentle agitation to separate epidermis from dermis. Dermal fragments were washed in HBSS/1% Pen/Strep, transferred into Collagenase A (Roche) solution, and processed as for lung EC isolation.

Human T cells were isolated from human peripheral blood using the Dynabeads Untouched Human T Cells kit (Thermo Fisher Scientific) according to the manufacturer's instructions and preactivated for 2–5 d in T cell medium (RPMI, 20% FCS, 2% glutamine, 1% penicillin/streptomycin, 1% Na-pyruvate, 1% nonessential amino acids, and 0.1% β-Mercaptoethanol) containing 10 ng/ml recombinant human IL2 (PeproTech) and 2 µg/ml Phytohemagglutinin-M (Roche). PMNs from human blood were isolated by density gradient centrifugation using Histopaque 1077 and 1119 (Sigma-Aldrich). The phase containing the granulocytes was removed, and cells were washed twice in wash buffer ($HBSS^{-/-}$, 25 mM Hepes, pH 7.3, and 10% FCS) before erythrocytes were lysed by incubation in 0.15 M NH_4Cl, 1 mM $KHCO_3$, and 0.1 mM Na_2EDTA for 4 min at room temperature. PMNs were used for transmigration assays directly after isolation.

The VE-PTP inhibitor AKB-9778 (Aerpio Therapeutics) was used as a 10 mM (6.07 mg/ml) stock solution in 5% glucose/H_2O. The following additional reagents were used: recombinant human TNF (PeproTech), IL-8 (R&D Systems), murine and human VEGF165 (PeproTech), human Thrombin (EMD Millipore), histamine (Sigma-Aldrich), COMP-Ang1 (G.Y. Koh), gelatin (Sigma-Aldrich), fluorescent mounting medium (Dako), 250-kD FITC-dextran (Sigma-Aldrich) and Dispase (Roche), 4-hydroxytamoxifen (Sigma-Aldrich), and tamoxifen (Sigma-Aldrich).

Antibodies. The following antibodies were used: pAb VE42 (Broermann et al., 2011) and pAb C5 against mouse VE-cadherin (Gotsch et al., 1997), pAb against human VE-cadherin (C-19; Santa Cruz Biotechnology, Inc.), murine pAb PTP 1–8 against the extracellular fibronectin type III–like domains 1–8 of VE-PTP (Winderlich et al., 2009), pAb VE-PTP-C against VE-PTP (Nawroth et al., 2002), mAb against PECAM-1 (1G5.1 and 5D2.6; Wegmann et al., 2006), pAb against PEC AM-1 (M-20; Santa Cruz Biotechnology, Inc.), mAb against N-cadherin (32/N-cadherin; BD), mAb against β-catenin (14/β-catenin; BD), mAb against plakoglobin (15/γ-catenin; BD), mAb against α-catenin (5/α-catenin; BD), mAb against p120-catenin (98/pp120; BD), pAb against β-catenin (Santa Cruz Biotechnology, Inc.), mAb against phosphotyrosine (4G10; Merck Millipore), mAb against α-tubulin (B-5-1-2; Sigma-Aldrich), mAb 3G1 against Tie-2 (Koblizek et al., 1997), mAb against human Tie-2 (Tek33.3; Merck Millipore), pAb

against pMLC-2 (Cell Signaling Technology), pAb against Claudin-5 (Invitrogen), pAb against NG2 (Merck Millipore), mAb against Rac1 (102/Rac1; BD), pAb against Rap1 (Merck Millipore), mAb against murine Endomucin (V7C7.1; Morgan et al., 1999), pAb against ICAM-1 (M-19; Santa Cruz Biotechnology, Inc.), mAb against human Tie-2 (D9D10; Cell Signaling Technology), pAb against Src-pY418 (Life Technologies), pAb against c-Src (SRC2; Santa Cruz Biotechnology, Inc.), mAb against VEGFR-2 (55B11; Cell Signaling Technology), and Phalloidin–Alexa Fluor 568 or –Alexa Fluor 647 (Invitrogen). Secondary antibodies were purchased from Dianova. Alexa Fluor 488–, Alexa Fluor 568–, and Alexa Fluor 647–coupled antibodies were purchased from Invitrogen.

Generation of conditional *Cdh5* gene–inactivated mice. *Cdh5*$^{lox/lox}$ mice were generated by flanking the ATG-containing exon 2 with loxP sites and inserting a neomycin selection cassette (flanked by Frt sites) upstream of the 3′ loxP site by homologous recombination of mouse embryonic stem cells. The targeting vector contained a 6.9-kb-long arm 5′ of exon 2 and the loxP site–flanked exon 2, followed by an FRT-flanked neo cassette and a 1.5-kb short arm. Neomycin-resistant clones were screened by PCR and Southern blot analysis. Positive embryonic stem cell clones were injected into blastocysts of C57BL/6 mice to generate chimeras, which were mated with C57BL/6 mice. The FRT-flanked neo cassette was excised by breeding with mice expressing Flp recombinase. To inactivate *Cdh5* in postnatal ECs, *Cdh5*$^{lox/lox}$ mice were bred to tamoxifen-inducible *Cdh5*(PAC)-Cre^{ERT2} (*Cdh5-iCre*) transgenics (Wang et al., 2010), resulting in *Cdh5*^{iECKO} mice. Mice were generated in cooperation with Genoway (Lyon) and backcrossed on the C57BL/6 mice background for at least nine generations. The following primers were used for genotyping: RMCE_for (5′-GAAGAGCTTTCGGGCTGG AATGACC-3′) and RMCE_rev (5′-GGATGATATGGTA GCAGGTGTTGGGG-3′), generating a 520-bp PCR product for WT and a 565-bp PCR product in *Cdh5*$^{lox/lox}$ mice. In addition, genotyping for the Cre gene was performed using the primers Cre_for (5′-GCCTGCATTACCGGTCGA-3′) and Cre_rev (5′-GTGGCAGATGGCGCGGCA-3′), generating either a 700-bp or no product.

Generation of conditional *Ptprb* gene–inactivated mice. *Ptprb*$^{lox/lox}$ mice were generated by flanking exon 20 with loxP sites and inserting a neomycin resistance cassette (flanked by Frt sites) upstream of the 3′ loxP sites by homologous recombination in mouse embryonic stem cells. The targeting vector contained a 3.4-kb short arm 5′ of exon 20 and the loxP site–flanked exon 20 followed by the FRT site–flanked neo cassette and a 10.9-kb long arm. Generation of *Ptprb*$^{lox/lox}$ mice backcrossed on the C57BL/6 mice background was performed as described for the *Cdh5*$^{lox/lox}$ mice. To inactivate *Ptprb* in postnatal ECs, *Ptprb*$^{lox/lox}$ mice were bred to tamoxifen-inducible *Pdgfb-iCre* transgenics (Claxton et al., 2008), resulting in *Ptprb*^{iECKO} mice. Mice were backcrossed on the C57BL/6 mice background for at least nine generations. To confirm that Cre excision of exon 20 results in a functional null *Ptprb* allele, mice were bred to a *Pgk-Cre* driver line (Lallemand et al., 1998) that expressed Cre recombinase already at the one-cell embryo stage. The following primers were used for genotyping: A/B geno S4 (5′-TGAACCCT GAAGAGTCTCACGTCCTTAC-3′) and A/B geno AS3 (5′-GCCTGCATGTATGCCCACGAGAT-3′), generating a 1,290-bp PCR product for WT and a 1,440-bp PCR product in *Cdh5*$^{lox/lox}$ mice. All animal experiments were approved by the Landesamt für Natur, Umwelt und Verbraucherschutz Nordrhein-Westfalen. Animals were kept in a barrier facility under special pathogen–free conditions.

Tamoxifen treatment. For in vivo application, 100 mg tamoxifen was mixed with 100 µl ethanol and 5 ml peanut oil and dissolved for 30 min in a water bath at 37°C using ultrasound. 100 µl of this solution was injected i.p. into *Ptprb*^{iECKO} and *Cdh5*^{iECKO} mice daily for five consecutive days, and mice were used for assays 2 d later (*Cdh5*^{iECKO} mice) or 5 d later (*Ptprb*^{iECKO} mice). Primary ECs of *Cdh5*^{iECKO} mice were treated with 2 µM 4-hydroxytamoxifen, the active metabolite of tamoxifen, in culture medium for 2–3 d.

Immunofluorescence staining. For in vitro stainings, cells were seeded on fibronectin (HUVECs)- or gelatin (primary mouse ECs)-coated chamber slides (Lab-Tek, 8 wells, glass) and grown to confluence before they were stimulated as described previously (Schulte et al., 2011), washed with PBS, fixed with 4% PFA/PBS for 10 min at room temperature, and permeabilized using 0.5% Triton X-100/PBS for 5 min at room temperature, followed by blocking with 3% BSA for 1 h and incubation with primary antibodies. Primary antibodies were detected with Alexa Fluor 488–, Alexa Fluor 568–, or Alexa Fluor 64–coupled secondary antibodies. Fluorescence signals were detected using a confocal laser-scanning microscope (LSM 780 inverted microscope; Carl Zeiss). For skin whole mount stainings, ears of mice were cut off at the base, and initial fixation for 10 min with 4% PFA in PBS was performed before they were split into halves. Staining on ear halves was performed as previously described for Cremaster (Schulte et al., 2011).

Immunohistochemistry. For histological examination of lung paraffin sections, mice were anesthetized using ketamine/xylazine. After lung perfusion with PBS, mice were intubated and lungs were inflated with 1 ml of 4% PFA/PBS. The trachea was tied, and lung and heart were removed en bloc and fixed in 4% PFA/PBS over night at 4°C. Afterward, the heart was removed, and the lung was cut into lobes, dehydrated, embedded in paraffin, and sectioned at 5 µm using a microtome. Sections were mounted on slides (Superfrost Plus; Menzel), dewaxed, rehydrated, and immunostained for endomucin using the antibody V7C7.1 as described previously (Brachtendorf et al., 2001) using the VECTASTAIN Elite

ABC kit (Vector Laboratories) to detect the primary antibodies. Counterstain was performed using Mayer's hematoxylin.

Electron microscopy. For electron microscopy, mice were anesthetized using ketamine/xylazine, and the body circulation was perfused first with 10 ml PBS via a peristaltic pump, followed by 40 ml of 2% paraformaldehyde and 2% glutaraldehyde in 0.1 M cacodylate buffer, pH 7.2. The tissues were removed and post-fixed in reduced 1% osmium tetroxide containing 1.5% potassium hexacyanoferrate. Subsequently, samples were dehydrated and embedded in epon. 60-nm ultrathin sections were cut on an ultramicrotome (UC6; Leica), counterstained with uranyl and lead, and imaged on an electron microscope (Tecnai-12-biotwin; FEI). All vessels were analyzed in the area of the section (~1 mm × 1 mm) and imaged for junction integrity (MegaView; Olympus). Furthermore, representative pictures of selected areas were imaged on high-resolution pictures with Ditabis plates.

Immunoprecipitation and immunoblotting. For coimmunoprecipitations, cells were lysed in lysis buffer (20 mM imidazole, pH 6.8, 100 mM NaCl, 2 mM $CaCl_2$, 1% Triton X-100, 0.04% NaN_3, and 1× complete EDTA-free protease inhibitors [Roche]). For detection of phospho-tyrosine after immunoprecipitation, cells were lysed in lysis buffer containing 20 mM Tris-HCl, pH 7.4, 150 mM NaCl, 2 mM $CaCl_2$, 1 mM Na_3VO_4, 1% Triton X-100, 0.04% NaN_3, and 1× complete EDTA-free protease inhibitors (Roche). For immunoprecipitation of proteins from mouse lung lysates, lungs were homogenized with an Ultra Turrax (IKA-Werke) in RIPA buffer containing 1% NP-40, 1% sodium deoxycholate, 0.01 M NaPi, 150 mM NaCl, 2 mM EDTA, 1 mM Na_3VO_4, and 2× Complete EDTA-free protease inhibitors, followed by incubation for 4 h at 4°C. Lysates were centrifuged at 4°C for 1 h at 20,000 *g*, and then aliquots were set aside for direct blot analysis, and aliquots for immunoprecipitation were precleared for 2 h at 4°C with protein A/G–Sepharose and subsequently incubated for 3 h at 4°C with protein A/G–Sepharose loaded with the respective antibodies. Immunocomplexes were washed five times with lysis buffer and analyzed by SDS-PAGE. Total cell or organ lysates or immunoprecipitated material was separated by SDS-PAGE and transferred to nitrocellulose (Schleicher & Schuell) by wet blotting. Blots were analyzed as described previously (Ebnet et al., 2000). For detection of phosphorylated tyrosine, milk powder in the blocking buffer was replaced by 2% BSA, and 200 µM Na_3VO_4 was added.

Rac1 activation assay. HUVECs were serum starved for 3 h before stimulation with vehicle, 6 µM AKB-9778, or 200 ng/ml COMP-Ang1 for 30 min. Then cells were lysed and a G-Lisa Rac1 activation assay was performed according to the manufacturer's protocol (G-LISA Rac1 Activation Assay Biochem kit Luminescence format; Cytoskeleton, Inc.). In brief, lysates were cleared by centrifugation at 14,000 rpm at 4°C for 2 min before protein concentrations were equalized, followed by incubation in a Rac-GTP affinity plate for 30 min. Next, the levels of GTP-loaded Rac1 proteins were detected by Rac1 antibodies and HRP-labeled secondary antibodies, and luminescence was measured in a 96-well plate reader (Synergy 2; BioTek).

Pull-downs of Rac1 and Rap1. For GST pull-downs of Rac1 or Rap1, cells were serum starved for 2–4 h before stimulation with vehicle, AKB-9778, or COMP-Ang1 for 30 min, followed by lysis in 50 mM Tris/HCl, pH 7.5, 1% Triton X-100, 100 mM NaCl, 10 mM $MgCl_2$, 5% glycerol, and protease inhibitors for 10 min. Lysates were centrifuged at 14,000 rpm and 4°C for 10 min and incubated with either Rac1 Assay Reagent (PAK-PBD-GST Beads; Cytoskeleton, Inc.) for a pull-down of Rac1 or Rap1 Assay Reagent (Ral-GDS-RBD Beads; Merck Millipore) for a pull-down of Rap1 for 45 min at 4°C in an overhead shaker. Beads were washed four times with lysis buffer and, together with aliquots of total lysates, subjected to immunoblot analysis with antibodies for Rac1 or Rap1.

RNA interference. For in vitro RNA interference of Tie-2, the siRNA 5′-TCGGTGCTACTTAACAACTTA-3′ (human Tie-2; QIAGEN) was used. For RNA-mediated interference of Rap1 expression in HUVECs, the following siRNAs were used in combination: 5′-GCAAGACAGTGGTGTAACT-3′ (human Rap1A) and 5′-GGACAAGGATTTGCATTAG-3′ (human Rap1B). As a negative control, siRNA that does not target any known mammalian gene was used (5′-UUC UCCGAACGUGUCACGU-3′; QIAGEN). Routinely, 10^6 HUVECs were transfected with 3 or 4 µg siRNA, respectively, using either nucleofection (Amaxa Biosystems) or INT ERFERin (Polyplus Transfection) according to the manufacturer's instructions. Cells were analyzed 48 h (Tie-2 siRNA) or 72 h (Rap1A/B siRNA) after transfection.

For RNA interference of Tie-2 in vivo, the siRNA 5′-CAGGAAGGTATGAGTACAAAT-3′ was used. The sequence was provided by QIAGEN, tested in vitro, and modified for higher stability for in vivo applications by Dharmacon (*siSTABLE*; GE Healthcare). As a negative control, siRNA that does not target any known mammalian gene was used that was modified identically (5′-TAGCGACTAAACACATCAA-3′; *siSTABLE*; GE Healthcare). Mice were injected i.v. with 60 µg siRNA using in vivo-jetPEI as transfer reagent (Polyplus Transfection) according to the manufacturer's instructions and analyzed 48 h later.

In vivo permeability assay in skin. 1 h before the assay, mice were injected subcutaneously with vehicle or AKB-9778 (0.6 mg per injection). Then, a modified Miles assay for the induction of vascular permeability in the skin was performed as described previously (Mamluk et al., 2005). For each assay, four to five 8–12-wk-old female mice were used. Evans blue dye (Sigma-Aldrich) was injected into the tail vein (100 µl of

a 1% solution in PBS), and after 15 min, 50 µl PBS, 100 ng murine VEGF165 in 50 µl PBS, or 225 ng histamine in 50 µl PBS was injected intradermally into the shaved back skin. Then, 30 min later, skin areas were excised and extracted with formamide for 5 d, and the concentration of the dye was measured at 620 nm with a spectrophotometer (Shimadzu).

In vivo LPS-induced lung permeability assay. 1 h before the assay, mice were injected subcutaneously with vehicle or AKB-9778 (0.6 mg per injection). To induce lung permeability, mice were exposed for 40 min to nebulized LPS (250 µg/ml *Salmonella* enteritidis; Sigma-Aldrich) or saline as a control. 4 h later, mice were i.v. injected with Evans blue and 5 min (for $Cdh5^{lox/lox}/Cdh5^{iECKO}$ mice) or 15 min (for control/Tie-2 siRNA–injected mice) later sacrificed, and the lung circulation was perfused. Lungs were removed and extracted with formamide for 5 d, and the concentration of the dye was measured at 620 nm with a spectrophotometer (Shimadzu).

In vivo permeability assay of inner organs. Mice were i.v. injected with Evans blue and 30 min later sacrificed, and the body circulation was perfused. Organs of interest were removed and extracted with formamide for 5 d, and the concentration of the dye was measured at 620 nm with a spectrophotometer (Shimadzu).

In vivo LPS-induced pulmonary inflammation. 1 h before the assay, mice were injected subcutaneously with vehicle or AKB-9778 (0.6 mg per injection). LPS-induced pulmonary inflammation was achieved as previously described (Zarbock et al., 2009). In brief, LPS from 500 µg/ml *Salmonella* enteritidis (Sigma-Aldrich) was nebulized, and mice were exposed for 45 min to nebulized LPS or saline as a control. 4 h later, mice were sacrificed and the lungs were lavaged with PBS. Leukocyte counts in the bronchoalveolar lavage fluid were analyzed, and the numbers of neutrophils were determined by FACS.

In vitro permeability assay. To determine paracellular permeability, 1.5×10^4 or 4×10^4 HUVECs were seeded on 100 µg/ml fibronectin–coated Transwell filters (Costar 3413, 0.4-µm pore size; Corning) and grown to confluence. For stimulation, HUVECs were starved for 2–4 h with EMB-2 containing 1% BSA, then preincubated with 200 ng/ml COMP-Ang1, 6–12 µM AKB-9778, 100 µg/ml anti–human hPTPβ antibody, or control reagents for 30 min, followed by stimulation with 1–2 U/ml thrombin (for 30 min) or 200 ng/ml VEGF165 (for 2 h) parallel to the diffusion of 0.25 mg/ml FITC-dextran (250 kD; Sigma-Aldrich) at 37°C and 10% CO_2. Fluorescence in the lower chamber was measured with a fluorimeter (Fluoromax-2; Jobin-Yvon), and monolayer integrity was confirmed by immunofluorescence staining for VE-cadherin after each assay.

In vitro transmigration assay. To analyze transendothelial migration of PMNs or T cells across HUVEC monolayers, HUVECs were grown to confluence on fibronectin-coated transwell filters (5-µm pore size; Corning) and stimulated with 5 nM TNF 15 h before the assay and treated either with 5 µM AKB-9778 or vehicle. For the assay, 2.5×10^5 human PMNs or T cells were allowed to transmigrate for 30 min toward the chemokine IL-8 (for PMNs) or SDF-1α (for T cells). Transmigrated leukocytes were counted using a CASY Cell Counter TT+ (Roche).

Statistical analysis. Datasets were tested for normality (Shapiro-Wilk) and equal variance. Statistical significance was analyzed using the one-way ANOVA test for independent samples or Mann-Whitney rank sum test. SigmaPlot 11 software was used for this analysis. P-values are indicated by asterisks: *, $P \leq 0.05$; **, $P < 0.01$; and ***, $P < 0.001$. Results are shown as means ± SEM. Immunoblot signals were quantified using the software Multi-Gauge V3.2 (Fuji). For immunoprecipitations, phospho-tyrosine signals were normalized to the levels of the precipitated protein.

ACKNOWLEDGMENTS

This work was supported in part by funds from the Max Planck Society (to D. Vestweber) and the Deutsche Forschungsgemeinschaft (DFG; SFB629-B1 and SFB1009-A1 to D. Vestweber) and was performed within the DFG Excellence Cluster Cells in Motion and the Max Planck–The University of Tokyo Center for Integrative Inflammmology (D. Vestweber).

D. Vestweber serves on the Scientific Advisory Board for Aerpio Therapeutics. K. Peters is an employee of Aerpio Therapeutics. The authors declare no competing financial interests.

Submitted: 24 April 2015
Accepted: 16 October 2015

REFERENCES

Allingham, M.J., J.D. van Buul, and K. Burridge. 2007. ICAM-1-mediated, Src- and Pyk2-dependent vascular endothelial cadherin tyrosine phosphorylation is required for leukocyte transendothelial migration. *J. Immunol.* 179:4053–4064. http://dx.doi.org/10.4049/jimmunol.179.6.4053

Ando, K., S. Fukuhara, T. Moriya, Y. Obara, N. Nakahata, and N. Mochizuki. 2013. Rap1 potentiates endothelial cell junctions by spatially controlling myosin II activity and actin organization. *J. Cell Biol.* 202:901–916. http://dx.doi.org/10.1083/jcb.201301115

Bäumer, S., L. Keller, A. Holtmann, R. Funke, B. August, A. Gamp, H. Wolburg, K. Wolburg-Buchholz, U. Deutsch, and D. Vestweber. 2006. Vascular endothelial cell–specific phosphotyrosine phosphatase (VE-PTP) activity is required for blood vessel development. *Blood.* 107:4754–4762. http://dx.doi.org/10.1182/blood-2006-01-0141

Brachtendorf, G., A. Kuhn, U. Samulowitz, R. Knorr, E. Gustafsson, A.J. Potocnik, R. Fässler, and D. Vestweber. 2001. Early expression of endomucin on endothelium of the mouse embryo and on putative hematopoietic clusters in the dorsal aorta. *Dev. Dyn.* 222:410–419. http://dx.doi.org/10.1002/dvdy.1199

Breviario, F., L. Caveda, M. Corada, I. Martin-Padura, P. Navarro, J. Golay, M. Introna, D. Gulino, M.G. Lampugnani, and E. Dejana. 1995. Functional properties of human vascular endothelial cadherin (7B4/cadherin-5), an endothelium-specific cadherin. *Arterioscler. Thromb. Vasc. Biol.* 15:1229–1239. http://dx.doi.org/10.1161/01.ATV.15.8.1229

Broermann, A., M. Winderlich, H. Block, M. Frye, J. Rossaint, A. Zarbock, G. Cagna, R. Linnepe, D. Schulte, A.F. Nottebaum, and D. Vestweber. 2011.

Dissociation of VE-PTP from VE-cadherin is required for leukocyte extravasation and for VEGF-induced vascular permeability in vivo. *J. Exp. Med.* 208:2393–2401. http://dx.doi.org/10.1084/jem.20110525

Claxton, S., V. Kostourou, S. Jadeja, P. Chambon, K. Hodivala-Dilke, and M. Fruttiger. 2008. Efficient, inducible Cre-recombinase activation in vascular endothelium. *Genesis.* 46:74–80. http://dx.doi.org/10.1002/dvg.20367

Corada, M., M. Mariotti, G. Thurston, K. Smith, R. Kunkel, M. Brockhaus, M.G. Lampugnani, I. Martin-Padura, A. Stoppacciaro, L. Ruco, et al. 1999. Vascular endothelial-cadherin is an important determinant of microvascular integrity in vivo. *Proc. Natl. Acad. Sci. USA.* 96:9815–9820. http://dx.doi.org/10.1073/pnas.96.17.9815

David, S., C.C. Ghosh, A. Mukherjee, and S.M. Parikh. 2011. Angiopoietin-1 requires IQ domain GTPase-activating protein 1 to activate Rac1 and promote endothelial barrier defense. *Arterioscler. Thromb. Vasc. Biol.* 31:2643–2652. http://dx.doi.org/10.1161/ATVBAHA.111.233189

Dejana, E., and D. Vestweber. 2013. The role of VE-cadherin in vascular morphogenesis and permeability control. In The Molecular Biology of Cadherins. Progress in Molecular Biology and Translational Science. Vol. 116. F. van Roy, editor. Elsevier, Oxford. 119–144. http://dx.doi.org/10.1016/B978-0-12-394311-8.00006-6

Dominguez, M.G., V.C. Hughes, L. Pan, M. Simmons, C. Daly, K. Anderson, I. Noguera-Troise, A.J. Murphy, D.M. Valenzuela, S. Davis, et al. 2007. Vascular endothelial tyrosine phosphatase (VE-PTP)-null mice undergo vasculogenesis but die embryonically because of defects in angiogenesis. *Proc. Natl. Acad. Sci. USA.* 104:3243–3248. http://dx.doi.org/10.1073/pnas.0611510104

Ebnet, K., C.U. Schulz, M.-K. Meyer Zu Brickwedde, G.G. Pendl, and D. Vestweber. 2000. Junctional adhesion molecule interacts with the PDZ domain-containing proteins AF-6 and ZO-1. *J. Biol. Chem.* 275:27979–27988.

Fachinger, G., U. Deutsch, and W. Risau. 1999. Functional interaction of vascular endothelial-protein-tyrosine phosphatase with the angiopoietin receptor Tie-2. *Oncogene.* 18:5948–5953. http://dx.doi.org/10.1038/sj.onc.1202992

Fukuhara, S., A. Sakurai, H. Sano, A. Yamagishi, S. Somekawa, N. Takakura, Y. Saito, K. Kangawa, and N. Mochizuki. 2005. Cyclic AMP potentiates vascular endothelial cadherin-mediated cell-cell contact to enhance endothelial barrier function through an Epac-Rap1 signaling pathway. *Mol. Cell. Biol.* 25:136–146. http://dx.doi.org/10.1128/MCB.25.1.136-146.2005

Fukuhara, S., K. Sako, T. Minami, K. Noda, H.Z. Kim, T. Kodama, M. Shibuya, N. Takakura, G.Y. Koh, and N. Mochizuki. 2008. Differential function of Tie2 at cell–cell contacts and cell–substratum contacts regulated by angiopoietin-1. *Nat. Cell Biol.* 10:513–526. http://dx.doi.org/10.1038/ncb1714

Gamble, J.R., J. Drew, L. Trezise, A. Underwood, M. Parsons, L. Kasminkas, J. Rudge, G. Yancopoulos, and M.A. Vadas. 2000. Angiopoietin-1 is an antipermeability and anti-inflammatory agent in vitro and targets cell junctions. *Circ. Res.* 87:603–607. http://dx.doi.org/10.1161/01.RES.87.7.603

Gavard, J., V. Patel, and J.S. Gutkind. 2008. Angiopoietin-1 prevents VEGF-induced endothelial permeability by sequestering Src through mDia. *Dev. Cell.* 14:25–36. http://dx.doi.org/10.1016/j.devcel.2007.10.019

Giampietro, C., A. Taddei, M. Corada, G.M. Sarra-Ferraris, M. Alcalay, U. Cavallaro, F. Orsenigo, M.G. Lampugnani, and E. Dejana. 2012. Overlapping and divergent signaling pathways of N-cadherin and VE-cadherin in endothelial cells. *Blood.* 119:2159–2170. http://dx.doi.org/10.1182/blood-2011-09-381012

Goel, S., N. Gupta, B.P. Walcott, M. Snuderl, C.T. Kesler, N.D. Kirkpatrick, T. Heishi, Y. Huang, J.D. Martin, E. Ager, et al. 2013. Effects of vascular-endothelial protein tyrosine phosphatase inhibition on breast cancer vasculature and metastatic progression. *J. Natl. Cancer Inst.* 105:1188–1201. http://dx.doi.org/10.1093/jnci/djt164

Gong, H., J. Rehman, H. Tang, K. Wary, M. Mittal, P. Chaturvedi, Y.Y. Zhao, Y.A. Komarova, S.M. Vogel, and A.B. Malik. 2015. HIF2α signaling inhibits adherens junctional disruption in acute lung injury. *J. Clin. Invest.* 125:652–664. (published erratum appears in *J. Clin. Invest.* 2015. 125:1364) http://dx.doi.org/10.1172/JCI77701

Gotsch, U., E. Borges, R. Bosse, E. Böggemeyer, M. Simon, H. Mossmann, and D. Vestweber. 1997. VE-cadherin antibody accelerates neutrophil recruitment in vivo. *J. Cell Sci.* 110:583–588.

Hakanpaa, L., T. Sipila, V.M. Leppanen, P. Gautam, H. Nurmi, G. Jacquemet, L. Eklund, J. Ivaska, K. Alitalo, and P. Saharinen. 2015. Endothelial destabilization by angiopoietin-2 via integrin β1 activation. *Nat. Commun.* 6:5962. http://dx.doi.org/10.1038/ncomms6962

Hayashi, M., A. Majumdar, X. Li, J. Adler, Z. Sun, S. Vertuani, C. Hellberg, S. Mellberg, S. Koch, A. Dimberg, et al. 2013. VE-PTP regulates VEGFR2 activity in stalk cells to establish endothelial cell polarity and lumen formation. *Nat. Commun.* 4:1672. http://dx.doi.org/10.1038/ncomms2683

Koblizek, T.I., A.S. Runting, S.A. Stacker, A.F. Wilks, W. Risau, and U. Deutsch. 1997. Tie2 receptor expression and phosphorylation in cultured cells and mouse tissues. *Eur. J. Biochem.* 244:774–779. http://dx.doi.org/10.1111/j.1432-1033.1997.00774.x

Kooistra, M.R., M. Corada, E. Dejana, and J.L. Bos. 2005. Epac1 regulates integrity of endothelial cell junctions through VE-cadherin. *FEBS Lett.* 579:4966–4972. http://dx.doi.org/10.1016/j.febslet.2005.07.080

Lallemand, Y., V. Luria, R. Haffner-Krausz, and P. Lonai. 1998. Maternally expressed PGK-Cre transgene as a tool for early and uniform activation of the Cre site-specific recombinase. *Transgenic Res.* 7:105–112. http://dx.doi.org/10.1023/A:1008868325009

Mamluk, R., M. Klagsbrun, M. Detmar, and D.R. Bielenberg. 2005. Soluble neuropilin targeted to the skin inhibits vascular permeability. *Angiogenesis.* 8:217–227. http://dx.doi.org/10.1007/s10456-005-9009-6

Mammoto, T., S.M. Parikh, A. Mammoto, D. Gallagher, B. Chan, G. Mostoslavsky, D.E. Ingber, and V.P. Sukhatme. 2007. Angiopoietin-1 requires p190 RhoGAP to protect against vascular leakage in vivo. *J. Biol. Chem.* 282:23910–23918. http://dx.doi.org/10.1074/jbc.M702169200

Mellberg, S., A. Dimberg, F. Bahram, M. Hayashi, E. Rennel, A. Ameur, J.O. Westholm, E. Larsson, P. Lindahl, M.J. Cross, and L. Claesson-Welsh. 2009. Transcriptional profiling reveals a critical role for tyrosine phosphatase VE-PTP in regulation of VEGFR2 activity and endothelial cell morphogenesis. *FASEB J.* 23:1490–1502. http://dx.doi.org/10.1096/fj.08-123810

Mochizuki, N. 2009. Vascular integrity mediated by vascular endothelial cadherin and regulated by sphingosine 1-phosphate and angiopoietin-1. *Circ. J.* 73:2183–2191. http://dx.doi.org/10.1253/circj.CJ-09-0666

Monaghan-Benson, E., and K. Burridge. 2009. The regulation of vascular endothelial growth factor-induced microvascular permeability requires Rac and reactive oxygen species. *J. Biol. Chem.* 284:25602–25611. http://dx.doi.org/10.1074/jbc.M109.009894

Morgan, S.M., U. Samulowitz, L. Darley, D.L. Simmons, and D. Vestweber. 1999. Biochemical characterization and molecular cloning of a novel endothelial-specific sialomucin. *Blood.* 93:165–175.

Nawroth, R., G. Poell, A. Ranft, S. Kloep, U. Samulowitz, G. Fachinger, M. Golding, D.T. Shima, U. Deutsch, and D. Vestweber. 2002. VE-PTP and VE-cadherin ectodomains interact to facilitate regulation of phosphorylation and cell contacts. *EMBO J.* 21:4885–4895. http://dx.doi.org/10.1093/emboj/cdf497

Ngok, S.P., R. Geyer, M. Liu, A. Kourtidis, S. Agrawal, C. Wu, H.R. Seerapu, L.J. Lewis-Tuffin, K.L. Moodie, D. Huveldt, et al. 2012. VEGF and Angiopoietin-1 exert opposing effects on cell junctions by regulating the Rho GEF Syx. *J. Cell Biol.* 199:1103–1115. http://dx.doi.org/10.1083/jcb.201207009

Nitta, T., M. Hata, S. Gotoh, Y. Seo, H. Sasaki, N. Hashimoto, M. Furuse, and S. Tsukita. 2003. Size-selective loosening of the blood-brain barrier in

claudin-5–deficient mice. *J. Cell Biol.* 161:653–660. http://dx.doi.org/10.1083/jcb.200302070

Nottebaum, A.F., G. Cagna, M. Winderlich, A.C. Gamp, R. Linnepe, C. Polaschegg, K. Filippova, R. Lyck, B. Engelhardt, O. Kamenyeva, et al. 2008. VE-PTP maintains the endothelial barrier via plakoglobin and becomes dissociated from VE-cadherin by leukocytes and by VEGF. *J. Exp. Med.* 205:2929–2945. http://dx.doi.org/10.1084/jem.20080406

Orsenigo, F., C. Giampietro, A. Ferrari, M. Corada, A. Galaup, S. Sigismund, G. Ristagno, L. Maddaluno, G.Y. Koh, D. Franco, et al. 2012. Phosphorylation of VE-cadherin is modulated by haemodynamic forces and contributes to the regulation of vascular permeability in vivo. *Nat. Commun.* 3:1208. http://dx.doi.org/10.1038/ncomms2199

Post, A., W.J. Pannekoek, S.H. Ross, I. Verlaan, P.M. Brouwer, and J.L. Bos. 2013. Rasip1 mediates Rap1 regulation of Rho in endothelial barrier function through ArhGAP29. *Proc. Natl. Acad. Sci. USA.* 110:11427–11432. http://dx.doi.org/10.1073/pnas.1306595110

Saharinen, P., L. Eklund, J. Miettinen, R. Wirkkala, A. Anisimov, M. Winderlich, A. Nottebaum, D. Vestweber, U. Deutsch, G.Y. Koh, et al. 2008. Angiopoietins assemble distinct Tie2 signalling complexes in endothelial cell–cell and cell–matrix contacts. *Nat. Cell Biol.* 10:527–537. http://dx.doi.org/10.1038/ncb1715

Sakuraba, J., T. Shintani, S. Tani, and M. Noda. 2013. Substrate specificity of R3 receptor-like protein-tyrosine phosphatase subfamily toward receptor protein-tyrosine kinases. *J. Biol. Chem.* 288:23421–23431. http://dx.doi.org/10.1074/jbc.M113.458489

Schulte, D., V. Küppers, N. Dartsch, A. Broermann, H. Li, A. Zarbock, O. Kamenyeva, F. Kiefer, A. Khandoga, S. Massberg, and D. Vestweber. 2011. Stabilizing the VE-cadherin–catenin complex blocks leukocyte extravasation and vascular permeability. *EMBO J.* 30:4157–4170. http://dx.doi.org/10.1038/emboj.2011.304

Shen, J., M. Frye, B.L. Lee, J.L. Reinardy, J.M. McClung, K. Ding, M. Kojima, H. Xia, C. Seidel, R. Lima e Silva, et al. 2014. Targeting VE-PTP activates TIE2 and stabilizes the ocular vasculature. *J. Clin. Invest.* 124:4564–4576. http://dx.doi.org/10.1172/JCI74527

Taddei, A., C. Giampietro, A. Conti, F. Orsenigo, F. Breviario, V. Pirazzoli, M. Potente, C. Daly, S. Dimmeler, and E. Dejana. 2008. Endothelial adherens junctions control tight junctions by VE-cadherin-mediated upregulation of claudin-5. *Nat. Cell Biol.* 10:923–934. http://dx.doi.org/10.1038/ncb1752

Thurston, G., J.S. Rudge, E. Ioffe, H. Zhou, L. Ross, S.D. Croll, N. Glazer, J. Holash, D.M. McDonald, and G.D. Yancopoulos. 2000. Angiopoietin-1 protects the adult vasculature against plasma leakage. *Nat. Med.* 6:460–463. http://dx.doi.org/10.1038/74725

Turowski, P., R. Martinelli, R. Crawford, D. Wateridge, A.P. Papageorgiou, M.G. Lampugnani, A.C. Gamp, D. Vestweber, P. Adamson, E. Dejana, and J. Greenwood. 2008. Phosphorylation of vascular endothelial cadherin controls lymphocyte emigration. *J. Cell Sci.* 121:29–37. http://dx.doi.org/10.1242/jcs.022681

Vockel, M., and D. Vestweber. 2013. How T cells trigger the dissociation of the endothelial receptor phosphatase VE-PTP from VE-cadherin. *Blood.* 122:2512–2522. http://dx.doi.org/10.1182/blood-2013-04-499228

Wang, Y., M. Nakayama, M.E. Pitulescu, T.S. Schmidt, M.L. Bochenek, A. Sakakibara, S. Adams, A. Davy, U. Deutsch, U. Lüthi, et al. 2010. Ephrin-B2 controls VEGF-induced angiogenesis and lymphangiogenesis. *Nature.* 465:483–486. http://dx.doi.org/10.1038/nature09002

Wegmann, F., B. Petri, A.G. Khandoga, C. Moser, A. Khandoga, S. Volkery, H. Li, I. Nasdala, O. Brandau, R. Fässler, et al. 2006. ESAM supports neutrophil extravasation, activation of Rho, and VEGF-induced vascular permeability. *J. Exp. Med.* 203:1671–1677. http://dx.doi.org/10.1084/jem.20060565

Wessel, F., M. Winderlich, M. Holm, M. Frye, R. Rivera-Galdos, M. Vockel, R. Linnepe, U. Ipe, A. Stadtmann, A. Zarbock, et al. 2014. Leukocyte extravasation and vascular permeability are each controlled in vivo by different tyrosine residues of VE-cadherin. *Nat. Immunol.* 15:223–230. http://dx.doi.org/10.1038/ni.2824

Winderlich, M., L. Keller, G. Cagna, A. Broermann, O. Kamenyeva, F. Kiefer, U. Deutsch, A.F. Nottebaum, and D. Vestweber. 2009. VE-PTP controls blood vessel development by balancing Tie-2 activity. *J. Cell Biol.* 185:657–671. http://dx.doi.org/10.1083/jcb.200811159

Zarbock, A., M.R. Distasi, E. Smith, J.M. Sanders, G. Kronke, B.L. Harry, S. von Vietinghoff, K. Buscher, J.L. Nadler, and K. Ley. 2009. Improved survival and reduced vascular permeability by eliminating or blocking 12/15-lipoxygenase in mouse models of acute lung injury (ALI). *J. Immunol.* 183:4715–4722. http://dx.doi.org/10.4049/jimmunol.0802592